Takahashi K, Hayashi N, Kaminogawa S, and Ra C,	Molecular mechanisms for transcriptional regulation of human high-affinity IgE receptor β-chain gene induced by GM-CSF.	*J. Immunol.*	177	4605-4611	(2006)
Nakanishi Y, Murashima K, Ohara H, Suzuki T, Hayashi H, Sakamoto M, Fukasawa T, Kubota H, Hosono A, Kono T, Kaminogawa S, and Benno Y,	Increase in terminal fragments of 16S rRNA genes derived from *Bacteroidetes* after administration of short-chain fructooligosaccharides.	*Appl. Environ. Microbiol.*	72	6271-6276	(2006)
Tsuda M, Hosono A, Fujioka M, Hachimura S, Nakamura R, Hirayama K, Itoh K, and Kaminogawa S	The role of *Bifidobacterium* in the development of gut immune systems: analysis using gnotobiotic TCR-transgenic mice.	*Animal Cell Technology: Basic & Applied Aspects*	14	93-99	(2006)
Nakanishi Y, Hosono A, Kimura T, and Kaminogawa S	The role of $CD4^+$ T cells in IgA production in murine Peyer's patches following oral feeding of *Bifidobacterium* components.	*Animal Cell Technology: Basic & Applied Aspects*	14	101-106	(2006)
Suzuki T, Hosono A, Hachimura S, Suzuki T, and Kaminogawa S	Modulation of cytokine and immunoglobulin A release by beta-(1,3-1,6)-glucan from Aureobasidium pullulans strain 1A1.	*Animal Cell Technology: Basic & Applied Aspects*	14	369-375	(2006)
Kim JY, Lee S, Jeong DW, Hachimura S, Kaminogawa S, Lee HJ	In vivo immunopotentiating effects of cellular components from *Lactococcus lactis* ssp lactis.	*J. Microbiol. Biotechnol.*	16	786-790	(2006)
Suzuki S, Shimojo N, Tajiri Y, Kumemura M, and Kohno Y.	Differences in the composition of intestinal *Bifidobacterium* species and the development of allergic diseases in infants in rural Japan.	*Clin. Exp. Allergy*			(in press)
Kubota Y, Umegaki K, Kagota S, Tanaka N, Nakamura K, Kunitomo M, Shinozuka K	Evaluation of blood pressure measured by tail-cuff methods (without heating) in spontaneously hypertensive rats.	*Biol. Pharm. Bull.*	29(8)	1756-1758	(2006)
Kubota Y, Tanaka N, Kagota S, Nakamura K, Kunitomo M, Umegaki K, Shinozuka K.	Effects of Ginkgo biloba extract feeding on salt-induced hypertensive Dahl rats.	*Biol. Pharm. Bull.*	29(2)	266-269	(2006)

Kubota Y, Tanaka N, Kagota S, Nakamura K, Kunitomo M, Umegaki K, Shinozuka K,	Effects of Ginkgo biloba extract on blood pressure and vascular endothelial response by acetylcholine in spontaneously hypertensive rats.	*J. Pharm. Pharmacol.,*	58(2)	243-249	(2006)
Kagota S, Yamaguchi Y, Tanaka N, Kubota Y, Kobayashi K, Nejime N, Nakamura K, Kunitomo M, Shinozuka K,	Disturbances in nitric oxide/cyclic guanosine monophosphate system in SHR/NDmcr-cp rats, a model of metabolic syndrome.	*Life Sci.*	78(11)	1187-1196	(2006)
Saotome Y, Tada A, Hanada N, Yoshihara A, Uematsu H, Miyazaki H, and Senpuku H,	Relationship of cariogenic bacteria levels with periodontal status and root surface caries in elderly Japanese.	*Gerodontol.*	23(4)	219-225	(2006)
Kaneko N, Yoshihara A, Ida H, Nomura Y, Imai S, Nisizawa T, Sakuma S, Hanada N, and Miyazaki H,	Influence of a fluoride mouthrinse on mutans streptococci in schoolchildren.	*Caries Res.*	40(6)	501-507	(2006)
Tamaki Y, Nomura Y, Takeuchi H, Ida H, Arakawa H, Tsurumoto A, Kumagai T, and Hanada N,	Study of the clinical usefulness of a dental drug system for selective reduction of mutans streptococci using a case series.	*J. Oral Sci.,*	48(3)	111-116	(2006)
Motegi M, Takagi Y, Yonezawa H, Hanada N, Terajima J, Watanabe H, and Senpuku H.	Assessment of genes associated with Streptococcus mutans biofilm morphology.	*Appl. Environ. Microbiol.*	72(9)	6277-6287	(2006)
Kamoda T, Imai T, Sato T, Imai S, Nisizawa T, and Hanada N.	Effect of disaccharide xylosylfructoside on sucrose cariogenicity in an artificial mouth system.	*J. Dental Health*	56	281-288	(2006)
岸光男, 高橋雅洋, 岸香代, 晴山婦美子, 田村光平, 阿部晶子, 杉浦剛,	口腔ケアの評価指標とreal-time PCRによる舌苔中細菌数との関連	口腔衛生学会誌	56(5)	665-672	(2006)

相澤文恵, 米満正美					
Nakajo K, Komori R, Ishikawa S, Ueno T, Suzuki Y, Iwami Y, Takahashi N.	Resistance to acidic and alkaline environments in the endodontic pathogen Enterococcus faecalis.	*Oral Microbiol. Immunol.*	21(5)	283-288	(2006)
Miyasawa-Hori H, Aizawa S, Takahashi N.	Difference in the xylitol sensitivity of acid production among Streptococcus mutans strains, and its biochemical mechanism.	*Oral Microbiol. Immunol.*	21(4)	201-205	(2006)
Sato R, Sato T, Takahashi I, Sugawara J, Takahashi N.	Profiling of bacterial flora in crevices around titanium orthodontic anchor plates.	*Clin. Oral Implants Res.*	18(1)	21-26	(2007)
Mitani H, Takahashi I, Onodera K, Bae J-W, Sato T, Takahashi N, Sasano Y, Igarashi K and Mitani H	Comparison of age-dependent expression of aggrecan and ADAMTSs in mandibular condylar cartilage, tibial growth plate, and articular cartilage in rats.	*Histochem Cell Biol*	126(3)	371-380	2006
Shimonishi M, Takahashi N, Komatsu M.	*In vitro* differentiation of epithelial cells cultured from human periodontal ligament.	*J Periodontal Res*	42	in press	2007
佐藤充太、 下西充、 高橋信博、 小松正志	培養ヒト歯根膜細胞由来上皮細胞と線維芽細胞の境界面におけるオステオポンチンおよびオステオカルシンの発現	*日歯保存誌*	49(1)	92-98	2006

Food antigen causes T_H2-dependent enteropathy followed by tissue repair in T-cell receptor transgenic mice

Haruyo Nakajima-Adachi, PhD,[a] Ayumi Ebihara, MS,[a] Akira Kikuchi, MS,[a] Tsuyoshi Ishida, MD,[b] Kiyomi Sasaki, BS,[a] Kiyomi Hirano,[c] Hiroko Watanabe, PhD,[d] Kazumi Asai, PhD,[a] Yoshimasa Takahashi, PhD,[e] Yutaka Kanamori, MD,[f] Naoki Shimojo, MD, PhD,[c] Hiroshi Matsuda, DVM, PhD,[g] Yoichi Kohno, MD, PhD,[c] Satoshi Hachimura, PhD,[a] and Shuichi Kaminogawa, PhD[h] *Tokyo, Chiba, and Kanagawa, Japan*

Background: Clarification of the mechanisms underlying the development of food-sensitive intestinal inflammation will provide an important clue to combating food allergies.
Objective: To establish a model of intestinal inflammation caused by oral administration of antigen without additional treatments, we focused on the ovalbumin (OVA) 23-3 T-cell receptor transgenic mouse, which had been reported to have high serum antigen-specific IgE responses to the feeding of an egg white diet.
Methods: Changes in body weight of mice fed an egg white diet were monitored throughout the 28-day experimental period. After the 28-day feeding, intestinal tissues were harvested for histologic examination. Endogenous production of cytokines and histamine in the jejunum, and production of cytokines secreted by OVA-specific $CD4^+$ T cells purified from mesenteric lymph nodes, were analyzed.
Results: Egg white diet–fed OVA23-3 mice developed weight loss and inflammation with villous atrophy and goblet cell hyperplasia, especially in the jejunum. A further characteristic feature was evidence of weight recovery and tissue repair. Jejunal inflammation was also observed in egg white diet–fed recombination activating gene (RAG)-2–deficient OVA23-3 mice. In addition, tissue sections revealed significant infiltration of specific IgE-positive cells and IgE-positive degranulating mast cells. Higher levels of IL-4 and significant levels of histamine were detected in the tissues. In the supernatant of OVA-stimulated T cells, IL-10 levels were also markedly elevated.
Conclusion: We report that high-dose and continuous intake of primitive OVA alone induces enteropathy containing regions under repair in OVA23-3 mice. Antigen-specific T cells and inflammatory cells primed by T_H2 responses play important roles in regulation of development and improvement of the disease.
Clinical implications: Long-term antigen intake causes T_H2-dependent and food-sensitive enteropathy followed by tissue repair. (J Allergy Clin Immunol 2006;117:1125-32.)

Key words: *T-cell receptor transgenic mouse, food-sensitive intestinal inflammation, ovalbumin, food antigen intake, antigen-specific T cells, IgE, mast cell, T_H2, histamine, tissue repair*

Several animal studies have been performed to clarify mechanisms underlying gastrointestinal hypersensitivities or allergies caused by food-derived antigen and to enhance progress toward diagnostic and/or protective measures against them.[1,2] In mouse models of food-sensitive intestinal inflammation, there are numerous examples of IgE-independent[3-7] and IgE-dependent models[8-10] but few of mixed models. Until now, almost all models have been established by using adjuvant-associated antigens, injection of drugs concurrent with dietary antigen, or microbial flora–associated antigen to promote systemic or local sensitization initially and to overcome antigen-induced oral tolerance.[2] However, these procedures do not clarify how the intestinal immune system regulates the induction of tolerance or of food-sensitive intestinal inflammation.

Our previous studies of food allergy prompted us to develop a mouse model of intestinal inflammation.[11,12] We focused on the transgenic mouse with a T-cell receptor (TCR) recognizing ovalbumin (OVA) residues 323-339[13] as a means of amplifying immunologic reactions to orally administered antigens without using adjuvant or other agents, because the mouse has been reported to have specific-IgE responses to the 28-day oral feeding with an egg white (EW) diet.[14] We have noticed that these mice had a trend toward loose feces after commencing the EW diet. Thus, we analyzed the histology of their mucosal and immunologic tissues and succeeded in developing a novel and unique mouse model.

From [a]the Department of Applied Biological Chemistry, Graduate School of Agricultural and Life Sciences, University of Tokyo; [b]the Department of Diagnostic Pathology, Kanto Medical Center Nippon Telegraph and Telephone East Corporation, Tokyo; [c]the Department of Pediatrics, Chiba University; [d]the Chemistry Division, Kanagawa Prefectural Institute of Public Health; [e]the Department of Immunology, National Institute of Infectious Diseases, Tokyo; [f]the Department of Pediatric Surgery, University of Tokyo; [g]the Division of Animal Science, Graduate School, Institute of Symbiotic Science and Technology, Tokyo University of Agriculture and Technology; and [h]the Department of Food Science and Technology, Nihon University College of Bioresource Sciences, Kanagawa.

Disclosure of potential conflict of interest: The authors have declared that they have no conflict of interest.
Received for publication April 11, 2005; revised January 10, 2006; accepted for publication January 11, 2006.

Reprint requests: Haruyo Nakajima-Adachi, PhD, Department of Applied Biological Chemistry, Graduate School of Agricultural and Life Sciences, University of Tokyo, 1-1-1 Yayoi, Bunkyo-Ku, Tokyo 113-8657, Japan. E-mail: aryu@mail.ecc.u-tokyo.ac.jp.

0091-6749/$32.00

doi:10.1016/j.jaci.2006.01.016

Abbreviations used
AB: Alcian blue
BALB-mice: BALB/c mice
CN: Casein
CNB: Casein diet–fed BALB/c mice
DFS: Direct fast scarlet
EW: Egg white
EWB: Egg white diet–fed BALB/c mice
EWR: Egg white diet–fed RAG-2–deficient BALB/c mice
FITC: Fluorescein isothiocyanate
MLN: Mesenteric lymph nodes
OVA: Ovalbumin
PAS: Periodic acid-Schiff
TB: Toluidine blue
TCR: T-cell receptor
Tg-mice: Ovalbumin 23-3 mice

METHODS

Animals

Ovalbumin 23-3 mice transgenic for OVA323-339–specific and I-A^d–restricted TCR-αβ (Vα3/Vβ15) on a BALB/c genetic background were kindly provided by S. Habu (Tokai University School of Medicine).[13] These mice were crossed with recombination activating gene (RAG)-2–deficient BALB/c-mice (BALB-mice) to establish RAG-2–deficient OVA23-3 mice (Tg-mice). Animals were maintained in the Hoshino Animal Center (Chiba, Japan). Male mice were used because female mice did not show clear weight changes. Male BALB-mice were purchased from Clea Japan Inc (Tokyo, Japan). They were housed under specific pathogen-free conditions. Guidelines formulated by the University of Tokyo were followed for the care and use of animals.

Ovalbumin administration

Seven-week-old male Tg-mice, RAG-2–deficient BALB-mice, RAG-2–deficient Tg-mice, and BALB-mice were divided into experimental groups as indicated both in figures and figure legends and administered for 28 days with a range of experimental diets: CE2-diet (Clea Japan Inc), EW diet, OVA diet, or casein (CN) diet (Funabashi Farm, Funabashi, Japan). The composition of experimental diets is indicated in the Online Repository at www.jacionline.org. By feeding EW diet and OVA diet, it is calculated that a mouse consumes about 250 mg OVA per day. During the experimental period, the weight of each mouse was measured every 4 or 7 days. After the 28-day feeding, tissues were taken from each mouse for further analysis. Sera were obtained before and after feeding and stored at −80°C. Concentrations of serum total IgE and OVA-specific IgE, IgG_1, and IgG_{2a} were analyzed by ELISA and estimated as described previously.[14]

Histologic analysis

Longitudinal sections of intestinal tissue (3 cm) were taken from the duodenum, the jejunum (11 cm distal to duodenum), the ileum (the superior part of cecum), and the colon (proximal and distal), respectively. Tissues were opened longitudinally, fixed in 10%, formalin and embedded in paraffin. Sections 3 or 5 μm thick were prepared and stained with hematoxylin and eosin for morphologic analysis, direct fast scarlet (DFS) to analyze eosinophils, periodic acid-Schiff (PAS)–Alcian blue (AB) for visualization of goblet cells, and Toluidine blue (TB) to detect mast cells. Parameters and numbers of mice used for quantification of intestinal tissue inflammation are indicated in the Online Repository at www.jacionline.org. For analysis of inflammation by scanning electron microscopy, jejunal sections were fixed in 2.5% glutaraldehyde and coated with gold. Electron micrographs of these specimens were scanned by using an S-3500N scanning electron microscope (Hitachi, Tokyo, Japan) and stored for subsequent observation and analysis.

Immunohistochemical staining

Jejunum sections, 1 cm in length and 4 cm distal to duodenum, were mounted in optimal cutting temperature compound (Tissue-tek; Sakura, Tokyo, Japan). Cryosections (6 μm thick) were fixed with acetone at −20°C. After rehydration with PBS, sections were blocked overnight with antimouse CD16/CD32 Ab (2.4G2; Pharmingen, San Diego, Calif) at 4°C and stained overnight with fluorescein isothiocyanate (FITC)–conjugated rat antimouse IgE (R35-72; Pharmingen) or biotinylated rat antimouse IgE (R35-72; Pharmingen) at 4°C. Biotinylated sections were incubated with streptavidin–horseradish peroxidase (ZYMED, South San Francisco, Calif) followed by DAB (Sigma, St Louis, Mo). IgE-positive mast cells were detected by further counterstaining with TB. To detect ovalbumin-specific IgE, FITC-labeled sections were further stained with biotinylated OVA followed by streptavidin–Texas red (Roche, Tokyo, Japan).

Histamine and cytokine levels in whole gut tissue homogenates

Four-centimeter sections of the jejunum immediately distal to the duodenum were collected and processed according to the method of van Halteren et al.[15] Homogenates were centrifuged and supernatants used for determination of histamine levels by HPLC (Post-Colum Reaction Systems; Waters Co, Milford, Mass).[16] To study the endogenous production of IFN-γ, IL-4, and TNF-α, 6-cm sections of the jejunum located 5 cm distal to the duodenum were collected and processed. Protein lysates of the jejunum were prepared with a cocktail of proteinase inhibitors and centrifuged. Supernatants were collected and concentrations of IL-4 and IFN-γ assessed by ELISA as described previously.[14] The OptEIA ELISA Set was used for TNF-α analysis according to the manufacturer's instructions (Pharmingen). Histamine and cytokine contents were standardized to the weight of jejunum tissue in each sample.

Cell culture and cytokine measurements

Mesenteric lymph node (MLN) lymphocytes isolated from each mouse fed with the CN diet or EW diet were pooled for each experimental group. MLN $CD4^+$ T cells were positively identified by using anti-CD4 mAb conjugated to immunomagnetic beads and selected using a MACS cell separation system (Miltenyi Biotec, Bergish Gladbach, Germany) according to the manufacturer's protocol. The proportion of MLN $CD4^+$ T cells was more than 94% in each analysis. The MLN $CD4^+$ T cells (1×10^5 cells/well) were added to 96-well flat-bottom plates and cultured in the absence or presence of OVA (1 mg/mL) with mitomycin-treated splenocytes as antigen-presenting cells (4×10^5 cells/well) in complete RPMI 1640. Supernatants were collected 48 hours later and cytokine concentrations measured by ELISA (IFN-γ, IL-4, IL-2, and IL-5). The OptEIA ELISA Set was used for TNF-α and IL-10 analysis as described.

Statistical analysis

Results are presented as the means ± SDs. Weight change was analyzed by using the Fischer's Protect Least Significant Difference test of multiple comparisons. The Mann-Whitney *U* test was used for nonparametric analysis of levels of serum antibodies, histamine or

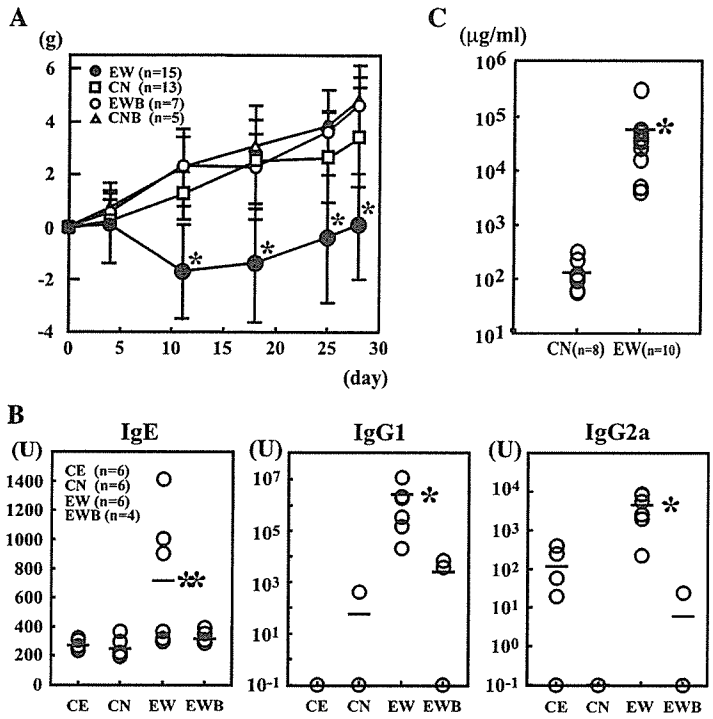

FIG 1. A, Weight loss in EW diet–fed Tg-mice. (*$P < .05$). **B,** Increase in serum OVA-specific antibodies in EW diet–fed Tg-mice. These data represent 4 independent experiments containing 3 to 6 mice in each group. **C,** Increase in total IgE in EW diet–fed Tg-mice. In *B and C,* ○ and bars indicate antibody titers for each mouse and the means, respectively. (*$P < .01$).

cytokine production, and the numbers of inflammatory cells in the intestine. Differences were considered statistically significant for values of $P < .05$.

RESULTS

Feeding of EW diet induces wasting diseases and hyperproduction of serum antibody in Tg-mice

Feeding Tg-mice with the EW diet caused loose feces (see this article's Fig E1 in the Online Repository at www.jacionline.org). Body weight changes from day 0 revealed that EW diet–fed Tg-mice (Fig 1, *A*: EW) failed to thrive from day 4, whereas from day 10 through day 28, weight loss was significant compared with control groups showing normal growth. However, body weights showed a tendency to recover after the initial loss. Control groups were composed of CE2 diet–fed Tg-mice (data not shown), CN diet–fed Tg-mice (Fig 1, *A*: CN), EW diet–fed BALB-mice (Fig 1, *A*: EWB), and CN diet–fed BALB-mice (Fig 1, *A*: CNB), respectively. There were no significant differences in volumes of experimental diet consumed by mice in each group (data not shown).

As shown in Fig 1, *B*, OVA-specific IgE was detected in some (but not all) EW diet–fed Tg-mice (Fig 1, *B*: EW). Extensive induction of OVA-specific IgG_1 and high levels of OVA-specific IgG_{2a} were detected in EW diet–fed Tg-mice compared with control groups (Fig 1, *B*: CN, EWB, and CE, CE2-diet-fed Tg-mice). All of the EW diet–fed Tg-mice (Fig 1, *C*: EW) showed significant total IgE responses compared with control group (Fig 1, *C*: CN).

Villous morphologic changes in the jejunum of EW diet–fed Tg-mice

Analysis of intestinal histology indicated that inflammation associated with morphologic changes was particularly noticeable in sections of the jejunum from EW diet–fed Tg-mice (Fig 2, *A*: EW). Changes to the jejunal tissue consisted of a thickened muscular layer, crypt elongation, and villous atrophy, associated with goblet cell hyperplasia and increased numbers of Paneth cells. However, the severity of inflammation varied from animal to animal in the 28-day feedings: inflammatory regions were identified on all sequential segments in some Tg-mice (Fig 2, *A*: EW-Jejunum; and Fig 2, *B*: EW1), and in discrete areas of sequential segments in others (partial villous atrophy, Fig 2, *B*: EW2). The severity of inflammation showing partial villous atrophy was moderate in general. A characteristic histologic feature in this inflammatory process is villous blunting of the mucosa. Villous blunting without significant inflammatory cell infiltration as indicated in these panels is considered to represent a moderate degree of inflammation under mucosal repair. Thus, these panels provide morphologic evidence of repair (Fig 2, *B*: EW3). PAS-AB staining confirmed excess mucus in EW diet–fed Tg-mice (Fig 2, *B*: EW1-PAS, PAS-AB–stained EW1).

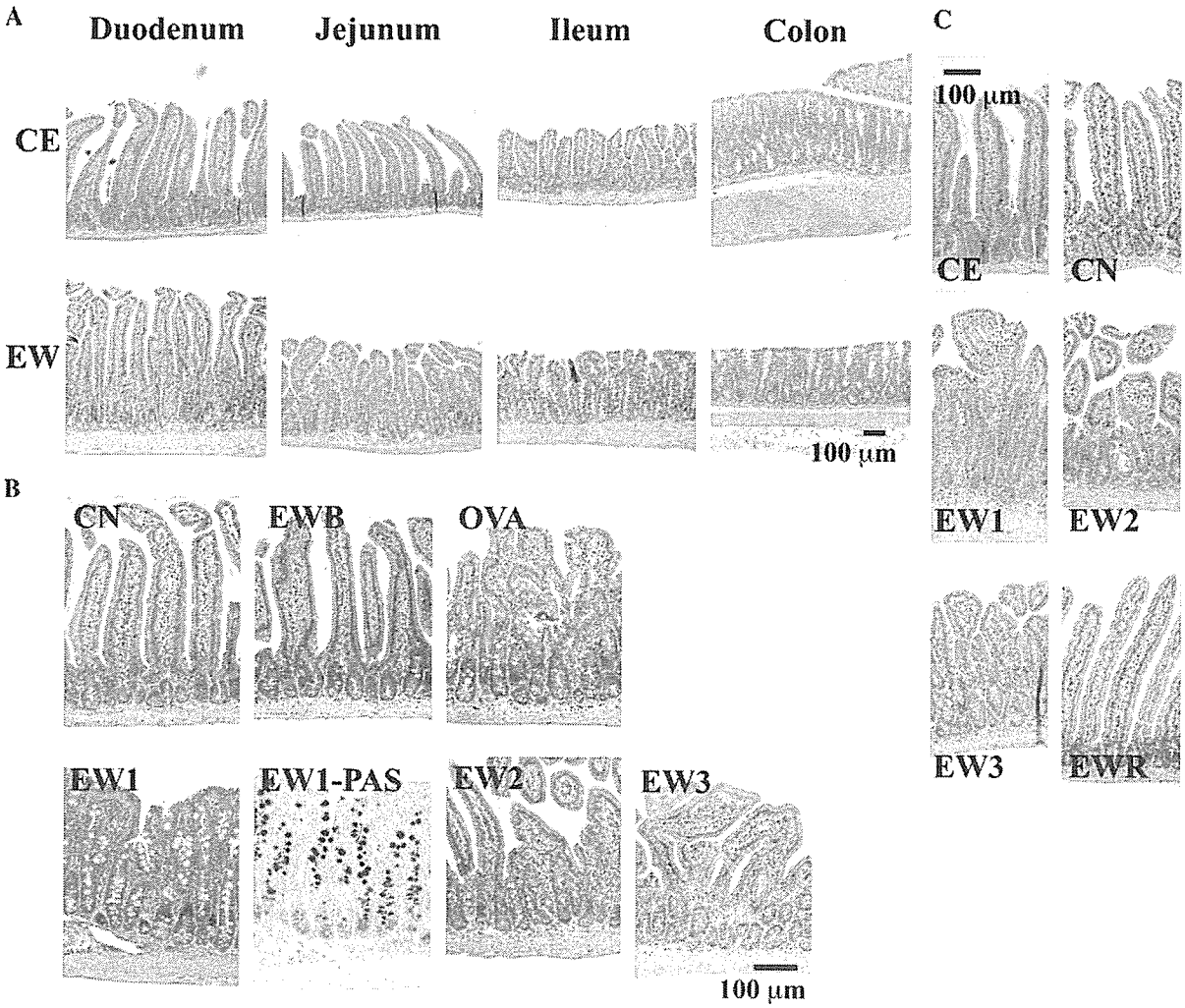

FIG 2. A, Intestinal inflammation detected in EW diet–fed Tg-mice. **B,** Detailed jejunal inflammation. EW1, EW2, and EW3 are panels from 3 different mice. **C,** Jejunal inflammation detected in EW diet–fed RAG-2–deficient Tg-mice (EW). EW1, EW2, and EW3 are panels from 3 different mice.

The duodenum and ileum from Tg-mice with severe inflammation in the jejunum also exhibited inflammation, which in most cases was less severe than that of the jejunum (Fig 2, *A*). Severe morphologic changes were not observed in the large intestine, although half of the sections from EW diet–fed Tg-mice (7 of 14 animals) showed polymorphonuclear leukocyte infiltration into the villous site of the lamina propria, particularly in the distal colon.

In OVA diet–fed Tg-mice, similar weight loss, increases in serum specific antibody titers, and inflammatory responses were observed (Fig 2, *B*: OVA; see also Figs E2, *A*, and E2, *B*, in the Online Repository at www.jacionline.org). This result indicated that the OVA diet has the same effects on the mouse as the EW diet, thereby showing that purified OVA, and not other components contained in EW, was the cause of the inflammation. Alterations to the intestinal mucosa could not be found in control groups (Fig 2, *A*: CE, CE2 diet–fed Tg-mice; Fig 2, *B*: CN, CN diet–fed Tg-mice; EWB, EW diet–fed BALB-mice, ovalbumin and CN diet–fed BALB-mice, data not shown).

We further analyzed the histology of EW diet–fed RAG-2–deficient Tg-mice. In these mice, severe weight loss (data not shown) along with jejunal inflammation were also observed (Fig 2, *C*: EW1, EW2, and EW3), but not in control groups (Fig 2, *C*: CE, CE2 diet–fed RAG-2–deficient Tg-mice; CN, CN diet–fed RAG-2–deficient Tg-mice; EWR, EW diet–fed RAG-2–deficient BALB-mice). RAG-2–deficient Tg-mice with developed disease are defective in local and serum IgE responses because of lack of mature B cells (data not shown),[17] and thereby have only OVA-specific T cells. On the other hand, RAG-2–deficient BALB-mice with undeveloped disease lack both mature B cells and T cells. The results thus indicate that specific T cells are indispensable in development of wasting disease and its pathogenesis in EW diet–fed Tg-mice.

The severity of the morphologic changes was reflected by the significant decrease in the villous height to crypt

depth in EW diet–fed Tg-mice. Scanning electron micrographs confirmed the results of hematoxylin and eosin staining experiments (see this article's Figs E3 and E4 in the Online Repository at www.jacionline.org).

Predominant T_H2 responses in EW diet–fed Tg-mice

Local cytokine production analysis in the jejunum showed higher levels of IL-4 but undetectable levels of IFN-γ (data not shown) in EW diet–fed Tg-mice (Fig 3, *A*: EW). IFN-γ was also not detected in the control group (CN diet–fed Tg-mice; data not shown). Significant differences in TNF-α production were not observed between EW diet–fed and CN diet–fed Tg-mice (Fig 3, *A*: CN).

The cytokines of OVA-specific $CD4^+$ T cells from MLN indicated significantly higher levels of IL-4 and IL-10 but significantly lower levels of IFN-γ production were detected in EW diet–fed Tg-mice (Fig 3, *B*: EW) compared with CN diet–fed Tg-mice (Fig 3, *B*: CN). IL-5 was below levels of detection in both groups. TNF-α and IL-2 production was significantly induced in CN diet–fed Tg-mice, whereas in EW diet–fed Tg-mice, both cytokines were at lower levels. Similar but lower production of cytokines of whole lymphocytes and undetectable levels in cells other than $CD4^+$ T cells obtained from MLN (data not shown) suggested that secretion of these cytokines depends on OVA-specific $CD4^+$ T cells in MLN.

Predominant infiltration of IgE-positive mast cells into the jejunum of EW diet–fed Tg-mice

We next investigated whether the higher titer of serum IgE responses in EW diet–fed Tg-mice was reflected in the prominent jejunal responses. IgE-positive mast cells, as well as other IgE-positive cells, predominantly infiltrated into the lamina propria near crypts or into submucosa of the jejunum of these mice (Fig 4, *A*: EW). Extensive degranulation was detected in most IgE-positive mast cells. Many of the IgE-positive cells in the villous lamina propria were predicted to be IgE-secreting plasma cells by further staining with antibody for CD138 (data not shown). An important result was detection of OVA-specific IgE-positive cells in the jejunum of EW-diet-fed Tg-mice (Fig. 4B), whereas IgE-positive cells and degranulation of mast cells were absent in the jejunum of control group (Fig 4, *A and C*: CN, CN diet–fed Tg-mice). Furthermore, local histamine levels in jejunal tissue of EW diet–fed Tg-mice (Fig 4, *C*: EW) were significantly increased compared with those of CN diet–fed Tg-mice, even there was considerable variation within each group. Thus, orally administered OVA induced mast cell degranulation triggered by binding of specific IgE to mast cells. The IgE-positive mast cells may therefore function by secreting large amounts of histamine. Analysis of paraffin embedded sections confirmed predominant infiltration of mast cells into the jejunum and distal colon of EW diet–fed Tg-mice compared with controls (see this article's Figs E5 and E6 and Results in Online Repository at www.jacionline.org), and the numbers were quantified (Fig 5).

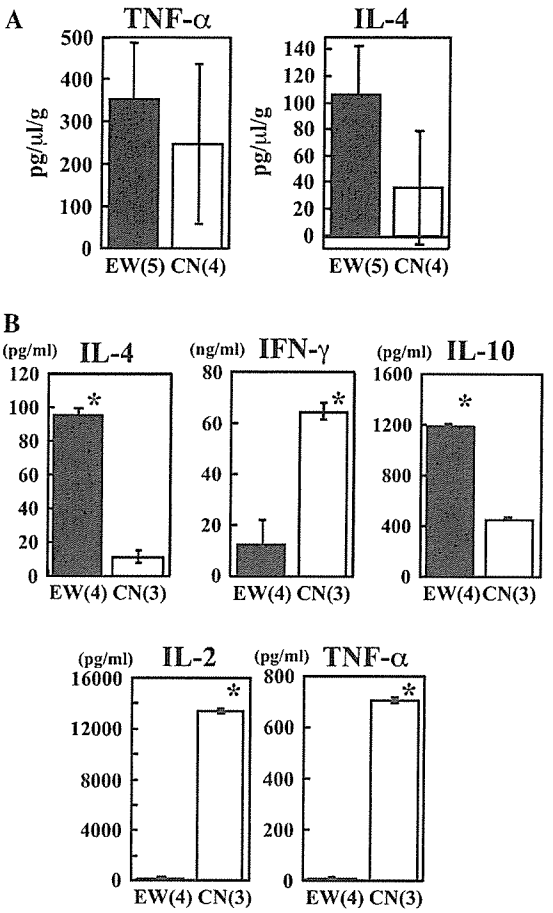

FIG 3. **A,** T_H2 polarized endogenous cytokine levels detected in the jejunum tissue from EW diet–fed Tg-mice. **B,** T_H2 polarized cytokines secreted by OVA-specific MLN $CD4^+$ T cells from EW diet–fed Tg-mice (*$P < .05$). The number of mice used in each group is indicated in *brackets;* results are representative of 2 independent experiments, respectively.

Other inflammatory responses in EW diet–fed Tg-mice

Participation of eosinophils or polymorphonuclear leukocytes in the inflammation process is indicated in the section "Aggregation of eosinophils in the lamina propria of the jejunum and distal colon and crypt abscess formation in the jejunum observed only in EW diet–fed Tg-mice" (see this article's Results and Figs E7 and E8 in Online Repository at www.jacionline.org). The average number of eosinophils aggregated in the villous lamina propria of the jejunum of EW diet–fed Tg-mice (Fig 6: EW) was significantly greater than that in control groups (Fig 6: CN, CN diet–fed Tg-mice; EWB, EW diet–fed BALB-mice). Inflammatory responses in other immunologic tissues and in tracheal tissue from EW diet–fed Tg-mice are described in the Methods and Fig E9 in the Online Repository at www.jacionline.org.

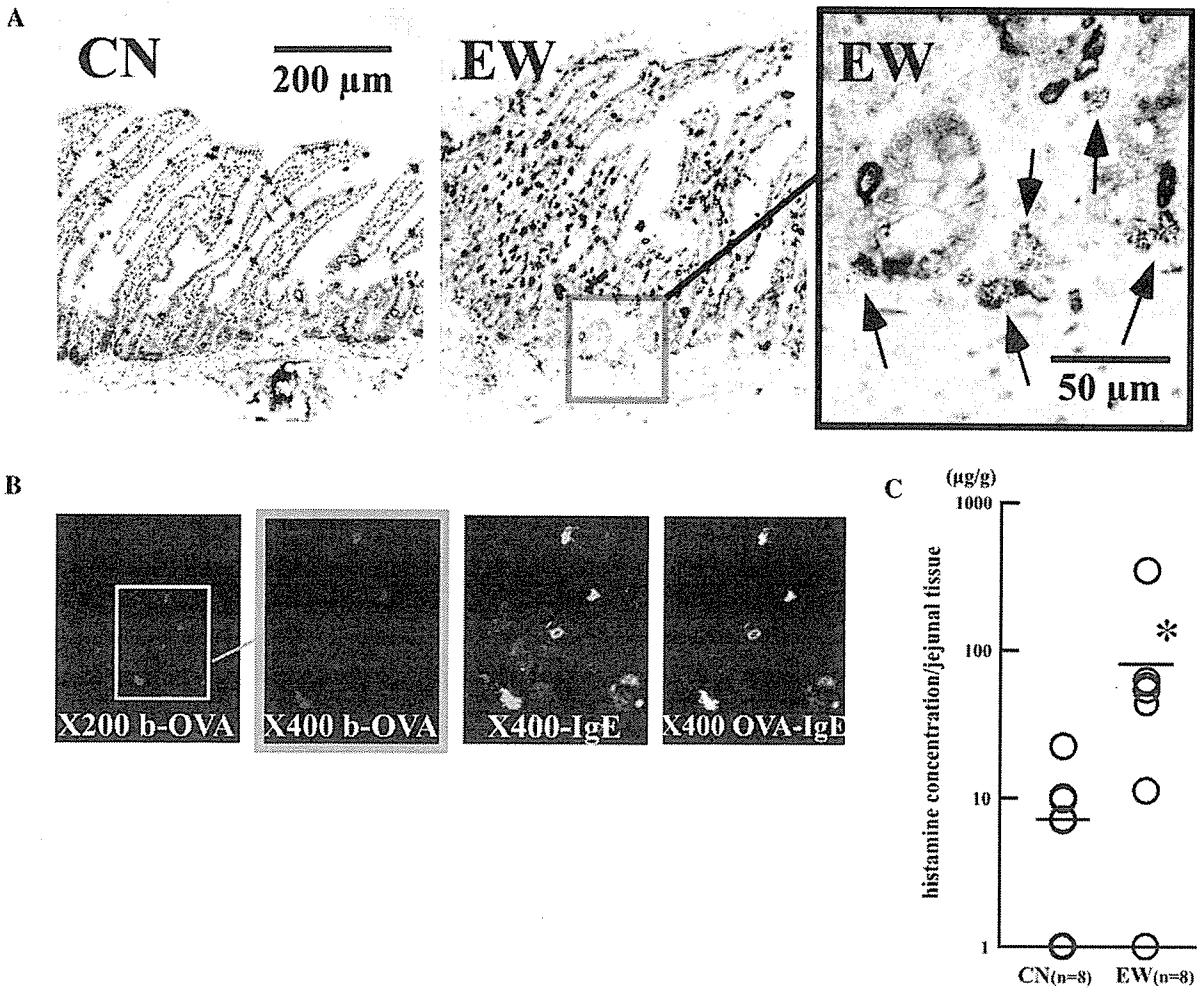

FIG 4. A, Mast cells bind IgE and degranulate in EW diet–fed Tg-mice. Arrows indicate IgE-positive and degranulating mast cells. **B,** Intestinal OVA-specific IgE detection in the jejunum of EW diet–fed Tg-mice. *b-OVA,* biotinylated OVA stained; *IgE,* FITC-labeled IgE-stained; *OVA-IgE,* double-stained with b-OVA and FITC-IgE. **C,** Jejunal histamine levels. ○, values of each mouse; —, means of the data. $*P < .05$).

DISCUSSION

We have successfully developed a unique animal model that undergoes weight loss in response to oral administration of OVA alone. The intestinal tissue of this animal model exhibits loss of villous architecture together with a characteristic feature of tissue repair, where specific IgE and degranulating IgE-positive mast cells, as well as antigen-specific T cells, were functional. Pathological changes were similar to results of studies on tissues collected from patients with food-sensitive enteropathy,[18-21] in that an increase in mucosal IgE secreting plasma cells and degranulating mast cells in the jejunum were described.[20] In addition, in relation to the large intestine, although this model lacked features such as diarrhea and morphologic changes observed in other models of food-induced colitis,[5-7] the pathology was consistent with that examined in tissues from patients with intestinal food allergies.[21] The deficiency in our model may be the absence of bacterial stimulation to initiate severe inflammation in the large intestinal immune system.

Pathological changes similar to those described by us showing loss of villous architecture in tissue from the ileum have been reported by Dohi et al,[22] who used a TCR-deficient mouse model to which IFN-γ–deficient $CD45RB^{high}$ T cells were transferred. In our model, established in an antigen-specific manner, it is unlikely that $CD45RB^{high}$ T cells would play a role in the development of inflammation. Also, inflammation in the model by Dohi et al[22] was detected at a different site from ours. However, wasting disease and villous atrophy are common results, and Dohi et al[22] further elucidated the significance of T_H2 cell responses. Thus, for our model, it is also considered that wasting disease and villous atrophy induced by feeding the EW diet would probably be mediated by significant T_H2-polarized responses. In food allergy reactions, T_H2 skewing has been demonstrated.[1] However it remains unclear whether the T_H2-type immune response stimulated by feeding with food allergens could

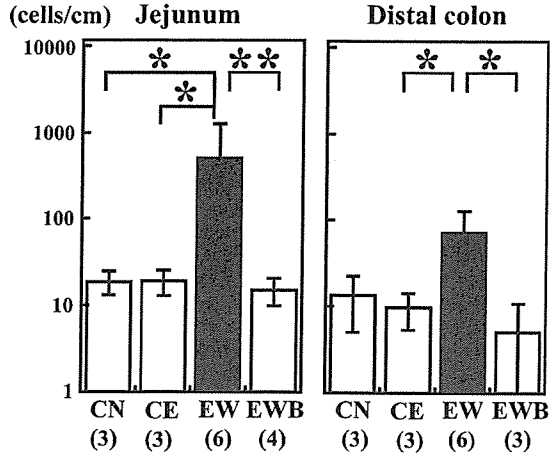

FIG 5. Quantification of mast cells predominantly infiltrating into the intestinal tissues of EW diet–fed Tg-mice (EW) compared with controls (CN or CE, CN diet–fed or CE2 diet–fed Tg-mice, respectively; EWB, EW diet–fed BALB-mice, $*P < .05$, $**P < .01$). The number of mice used in each group is indicated in *parentheses*.

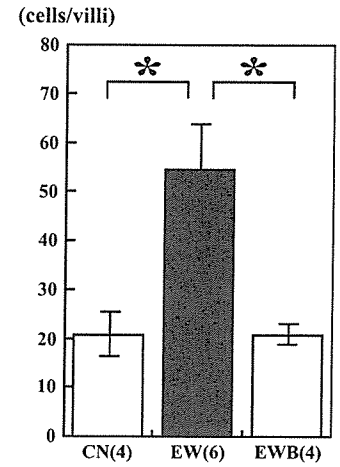

FIG 6. Quantification of eosinophils aggregated in the villous lamina propria of the jejunum from EW diet–fed Tg-mice. The number of mice used in each group is indicated in *parentheses*. ($*P < .01$).

explain the development of enteropathy observed in patients.[19] Although this is a mouse model, the current study is significant in showing that food-sensitive enteropathy relates to T_H2-dominant responses. Further detailed studies are needed to examine the involvement of IL-5 and IL-13 in our model, considering the eosinophil aggregation in villi and changes detected in the trachea.[23]

The most significant novel aspect of our model was that the histologic changes demonstrated a more complex pathology, as indicated particularly by the observation of the unsuccessful repair of injured tissues with marked infiltration of degranulating IgE-positive mast cells. The results of IgE-positive mast cell responses induced by food antigen intake can also be compared with findings reported by Brandt et al.[10] In their model, upregulation of OVA-specific T_H2-type responses by using aluminum hydroxide after oral administration of ovalbumin induced transient diarrhea dependent on IgE responses. This effect was induced by serotonin, not by histamine produced by mast cells. In contrast, elevated responses of serum and local IgE and the marked manifestation of mast cells in EW diet–fed Tg-mice in our study did not correlate with symptoms of diarrhea or the severity of villous atrophy. Furthermore, we have observed that even after an allergen-free period, oral readministration of either the EW diet or OVA itself to mice having higher levels of serum OVA-specific IgE did not cause diarrhea (data not shown). In addition, 10-day feeding with EW diet seemed to induce severe crypt elongation and goblet cell hyperplasia in all EW diet–fed Tg-mice (see this article's Fig E10: EW1 and EW2, in the Online Repository at www.jacionline.org). During this period, serum total IgE showed significantly low levels compared with those of the 28-day feeding.[14] Therefore, in contrast with the study by Brandt et al,[10] the dramatic infiltration of mast cells and IgE in our model for the 28-day feeding seemed to involve either the regulatory effect of histamine on T_H2 cells, or the predictive roles of IgE for oral tolerance binding to high expression of FcεRI on oral Langerhans cells,[24,25] rather than the injurious responses.

Actually in our system, the protective cytokine IL-10 was markedly produced in MLN $CD4^+$ T cells. Also, induction of oral tolerance has paradoxically been reported in spleen T cells from Tg-mice fed the EW diet for 28 days.[26] Thus, it is possible that the intestinal tissue, after exposure to an EW diet for 28 days, reflects a state of partial suppression of the injurious T_H2 responses, thereby causing the villous blunting or partial villous atrophy and a tendency to weight recovery. However, feeding times longer than 28 days, during the period serum IgE maintained higher levels, did not completely resolve inflammation in all mice, although the reason remained unclear (see this article's Fig E10: EW3 and EW4, in the Online Repository at www.jacionline.org). Further study of this animal model is expected to shed light on the mechanisms of T_H2-associated humoral and cellular activation in food-sensitive intestinal inflammation, thereby opening new possibilities for the treatment of food allergies involving tolerance induction.

We thank S. Habu and T. Sato at Tokai University for providing animals and K. Shida and S. Matsumoto at Yakult Central Institute for their technical support and for providing experimental systems and animals. We thank S. Fukuda at the University of Tokyo Hospital and K. Matsumoto at Hitachi High-Technologies Corp for their technical support with scanning electron microscopy. We thank C. Ogawa at Ochanomizu University for her technical support.

REFERENCES

1. Sampson HA, Sicherer SH, Birnbaum AH. AGA technical review on the evaluation of food allergy in gastrointestinal disorders. American Gastroenterological Association. Gastroenterology 2001;120:1026-40.
2. Helm RM. Food allergy animal models: an overview. Ann N Y Acad Sci 2002;964:139-50.

3. Ohtsuka Y, Yamashiro Y, Maeda M, Oguchi S, Shimizu T, Nagata S, et al. Food antigen activates intraepithelial and lamina propria lymphocytes in food-sensitive enteropathy in mice. Pediatr Res 1996;39:862-6.
4. Newberry RD, Stenson WF, Lorenz RG. Cyclooxygenase-2-dependent arachidonic acid metabolites are essential modulators of the intestinal immune response to dietary antigen. Nat Med 1999;5:900-6.
5. Iqbal N, Oliver JR, Wagner FH, Lazenby AS, Elson CO, Weaver CT. T helper 1 and T helper 2 cells are pathogenic in an antigen-specific model of colitis. J Exp Med 2002;195:71-84.
6. Yoshida M, Shirai Y, Watanabe T, Yamori M, Iwakura Y, Chiba T, et al. Differential localization of colitogenic Th1 and Th2 cells monospecific to a microflora-associated antigen in mice. Gastroenterology 2002;123: 1949-61.
7. Kweon MN, Yamamoto M, Kajiki M, Takahashi I, Kiyono H. Systemically derived large intestinal CD4(+) Th2 cells play a central role in STAT6-mediated allergic diarrhea. J Clin Invest 2000;106:199-206.
8. Ohtsuka Y, Naito K, Yamashiro Y, Yabuta K, Okumura K, Ra C. Induction of anaphylaxis in mouse intestine by orally administered antigen and its prevention with soluble high affinity receptor for IgE. Pediatr Res 1999;45:300-5.
9. Li XM, Schofield BH, Huang CK, Kleiner GI, Sampson HA. A murine model of IgE-mediated cow's milk hypersensitivity. J Allergy Clin Immunol 1999;103:206-14.
10. Brandt EB, Strait RT, Hershko D, Wang Q, Muntel EE, Scribner TA, et al. Mast cells are required for experimental oral allergen-induced diarrhea. J Clin Invest 2003;112:1666-77.
11. Nakajima H, Hachimura S, Nishiwaki S, Katsuki T, Shimojo N, Ametani A, et al. Establishment and characterization of alpha s1-casein-specific T-cell lines from patients allergic to cow's milk: unexpected higher frequency of CD8+ T-cell lines. J Allergy Clin Immunol 1996;97:1342-9.
12. Nakajima-Adachi H, Hachimura S, Ise W, Honma K, Nishiwaki S, Hirota M, et al. Determinant analysis of IgE and IgG4 antibodies and T cells specific for bovine alpha(s)1-casein from the same patients allergic to cow's milk: existence of alpha(s)1-casein-specific B cells and T cells characteristic in cow's-milk allergy. J Allergy Clin Immunol 1998;101: 660-71.
13. Sato T, Sasahara T, Nakamura Y, Osaki T, Hasegawa T, Tadakuma T, et al. Naive T cells can mediate delayed-type hypersensitivity response in T cell receptor transgenic mice. Eur J Immunol 1994;24:1512-6.
14. Shida K, Hachimura S, Ametani A, Ishimori M, Ling M, Hashiguchi M, et al. Serum IgE response to orally ingested antigen: a novel IgE response model with allergen-specific T-cell receptor transgenic mice. J Allergy Clin Immunol 2000;105:788-95.
15. van Halteren AG, van der Cammen MJ, Biewenga J, Savelkoul HF, Kraal G. IgE and mast cell response on intestinal allergen exposure: a murine model to study the onset of food allergy. J Allergy Clin Immunol 1997;99:94-9.
16. Yamanaka H, Matsumoto M. Simultaneous determination of polyamines in red meat fishes by high performance liquid chromatography and evaluation of freshness. J Food Hyg Soc Japan 1989;30:396-400.
17. Shinkai Y, Rathbun G, Lam KP, Oltz EM, Stewart V, Mendelsohn M, et al. RAG-2-deficient mice lack mature lymphocytes owing to inability to initiate V(D)J rearrangement. Cell 1992;68:855-67.
18. Maluenda C, Phillips AD, Briddon A, Walker-Smith JA. Quantitative analysis of small intestinal mucosa in cow's milk-sensitive enteropathy. J Pediatr Gastroenterol Nutr 1984;3:349-56.
19. Hauer AC, Breese EJ, Walker-Smith JA, MacDonald TT. The frequency of cells secreting interferon-gamma and interleukin-4, -5, and -10 in the blood and duodenal mucosa of children with cow's milk hypersensitivity. Pediatr Res 1997;42:629-38.
20. Shiner M, Ballard J, Smith ME. The small-intestinal mucosa in cow's milk allergy. Lancet 1975;1:136-4.
21. Dupont C, Heyman M. Food protein-induced enterocolitis syndrome: laboratory perspectives. J Pediatr Gastroenterol Nutr 2000;30:S50-7.
22. Dohi T, Fujihashi K, Koga T, Shirai Y, Kawamura YI, Ejima C, et al. T helper type-2 cells induce ileal villous atrophy, goblet cell metaplasia, and wasting disease in T cell-deficient mice. Gastroenterology 2003;124: 672-82.
23. Forbes E, Smart VE, D'Aprile A, Henry P, Yang M, Matthaei KI, et al. T helper-2 immunity regulates bronchial hyperresponsiveness in eosinophil-associated gastrointestinal disease in mice. Gastroenterology 2004; 127:105-18.
24. Akdis CA, Blaser K. Histamine in the immune regulation of allergic inflammation. J Allergy Clin Immunol 2003;112:15-22.
25. Allam JP, Novak N, Fuchs C, Asen S, Berge S, Appel T, et al. Characterization of dendritic cells from human oral mucosa: a new Langerhans' cell type with high constitutive FcεRI expression. J Allergy Clin Immunol 2003;112:141-8.
26. Asai K, Hachimura S, Kimura M, Toraya T, Yamashita M, Nakayama T, et al. T cell hyporesponsiveness induced by oral administration of ovalbumin is associated with impaired NFAT nuclear translocation and p27kip1 degradation. J Immunol 2002;169:4723-31.

Molecular Mechanisms for Transcriptional Regulation of Human High-Affinity IgE Receptor β-Chain Gene Induced by GM-CSF[1]

Kyoko Takahashi,*† Natsuko Hayashi,*‡ Shuichi Kaminogawa,† and Chisei Ra[2]*

The β-chain of the high-affinity receptor for IgE (FcεRI) plays an important role in regulating activation of FcεRI-expressing cells such as mast cells in allergic reactions. We already reported that the transcription factor myeloid zinc finger (MZF) 1 which formed a high m.w. complex including four and a half LIM-only protein (FHL)3 in the nucleus repressed human β-chain gene expression through an element in the fourth intron. We also found that GM-CSF induced expression of MZF-1 and nuclear translocation of FHL3. We screened a human cDNA library and identified NFY which was reported to bind histone deacetylases (HDACs) as a constituent of the complex. The C-subunit of NFY was demonstrated to form a ternary complex with MZF-1/FHL3 and interact with a β-chain gene region including the element in the fourth intron. HDAC1 and HDAC2 were also shown to interact with the fourth intron region of the β-chain gene. In a human mast cell line HMC-1 cultured with GM-CSF, both β-chain expression and acetylation of histones interacting with the fourth intron region of the β-chain gene were decreased. Collectively, these results indicated that HDACs, which were recruited to the β-chain gene through the element in the fourth intron by MZF-1/FHL3/NFY, repressed β-chain gene transcription by deacetylation of histones in the presence of GM-CSF. These mechanisms will be involved in not only the cell type-specific repression of β-chain gene expression in differentiating hemopoietic cells but also the repression of β-chain gene expression in the peripheral cells under specific circumstances. *The Journal of Immunology,* **2006, 177: 4605–4611.**

Cells of limited types such as mast cells, basophils, eosinophils (1), monocytes (2), Langerhans cells (3, 4), platelets (5, 6), and neutrophils (7) express the high-affinity receptor for IgE (FcεRI). FcεRI plays an important role in triggering IgE-mediated allergic reaction. Cross-linking of FcεRI on effector cells, for example mast cells, by Ag (allergen)-IgE complexes triggers allergic reaction by activating intracellular signal cascades to induce not only the release of chemical mediators in the early-phase reaction but also cytokine gene expressions leading to the late-phase reaction. Moreover, FcεRI on epidermal Langerhans cells in the skin is known to be involved in the Ag presentation by facilitating uptake of IgE-associated allergens, suggesting its pivotal role in the pathophysiology of atopic dermatitis.

FcεRI is composed of three different subunits, α, β, and γ, of which the α-chain directly binds IgE through its extracellular domain, while the β- and γ-chains are responsible for mediating intracellular signals. Although a functional receptor is expressed both as tetramers ($\alpha\beta\gamma_2$) and trimers ($\alpha\gamma_2$) in humans (8), intracellular signals (9, 10), in addition to cell surface expression of the receptor (11), were reported to be significantly amplified by β-chain, indicating that β-chain increases cell activation sensitivity to the stimulation by allergens. Recently, it was revealed that β-chain amplified degranulation and leukotriene secretion but suppressed cytokine production (12), indicating that β-chain regulates distinct intracellular signaling events in both positive and negative manners by the same molecule of itself. Furthermore, an alternative splice variant which encoded only an N-terminal portion of β-chain was found to be expressed in human mast cells (13). This truncation variant competed with full-length β and prevented FcεRI surface expression by inhibiting α-chain maturation (13). Because all of these findings indicate that β-chain is a fine regulator of FcεRI-mediated cell activation to precisely control the allergic reaction, elucidation of regulatory mechanisms of β-chain expression will make a meaningful contribution to medical intervention for allergy. In addition, because β-chain has only been reported to associate with FcγRIIIA except for FcεRI (14) and its expression is limited in the specific types of cells such as mast cells and basophils, applications which are targeted for β-chain are expected to exert cell type-specific effects.

The genomic structure of the human FcεRI β-chain gene was already determined (15), however, only a few analyses were performed on regulatory mechanisms of β-chain gene transcription. Two Oct-1-binding sites in the 5′ untranslated region were essential for activation of β-chain gene promoter (16). We revealed that the transcription factor myeloid zinc finger (MZF)[3] 1 repressed β-chain gene expression through an element in the fourth intron (17). It was suggested that this transcriptional repression required a cofactor; we therefore screened for MZF-1-binding proteins and

*Division of Molecular Cell Immunology and Allergology, Advanced Medical Research Center, Nihon University Graduate School of Medical Sciences, Tokyo, Japan; †Nihon University College of Bioresource Sciences, Kanagawa, Japan; and ‡Department of Applied Biological Chemistry, Tamagawa University, Tokyo, Japan

Received for publication March 15, 2006. Accepted for publication July 14, 2006.

The costs of publication of this article were defrayed in part by the payment of page charges. This article must therefore be hereby marked *advertisement* in accordance with 18 U.S.C. Section 1734 solely to indicate this fact.

[1] This work was supported in part by a Grant-in Aid from the Ministry of Education, Culture, Sports, Science, and Technology of Japan.

[2] Address correspondence and reprint requests to Dr. Chisei Ra, Division of Molecular Cell Immunology and Allergology, Advanced Medical Research Center, Nihon University Graduate School of Medical Sciences, 30-1 Oyaguchi Kamimachi, Itabashi-ku, Tokyo 173-8610, Japan. E-mail address: fcericra@med.nihon-u.ac.jp

[3] Abbreviations used in this paper: MZF, myeloid zinc finger; FHL, four and a half LIM-only protein; HDAC, histone deacetylase; BD, binding domain; ADH, alcohol dehydrogenase; HA, hemagglutinin; AD, activation domain; ChIP, chromatin immunoprecipitation.

0022-1767/06/$02.00

identified a four and a half LIM-only protein (FHL)3 as a repressive cofactor (18). FHL3 was predicted to act as an adaptor molecule recruiting unidentified other molecules to the MZF-1/DNA complex, because MZF-1 and FHL3 formed a very large m.w. complex in the nucleus (18). In contrast, GM-CSF was reported to induce MZF-1 expression (19). Moreover, we found that GM-CSF induced translocation of FHL3 from the cytoplasm to the nucleus (18), suggesting that both up-regulation of MZF-1 and nuclear translocation of FHL3 by GM-CSF facilitate formation of the MZF-1/FHL3 complex in the nucleus and reduce β-chain gene expression through the element in the fourth intron. It was actually reported that GM-CSF decreased FcεRI expression on the surface of a human mast cell line HMC-1 (20, 21). In this study, we report that FcεRI β-chain gene expression can be suppressed in the presence of GM-CSF through deacetylation of histones mediated by histone deacetylases (HDACs) which are recruited to the β-chain gene through the complex including MZF-1/FHL3.

Materials and Methods

Cell culture

HMC-1 (a human mast cell line) was cultured in IMDM (Invitrogen Life Technologies) at 37°C in a humidified incubator with 5% CO_2. KU812 (a human basophilic leukemia cell line) was cultured in RPMI 1640 (Sigma-Aldrich). Both media contained 10% (v/v) FBS (JRH Bioscience), 100 U/ml penicillin (Banyu Pharmaceutical), and 100 μg/ml streptomycin (Meiji Seika).

Plasmid construction

pBridge-MZF-1/FHL3 encoding human MZF-1 fused to GAL4 DNA binding domain (BD) under the constitutive alcohol dehydrogenase 1 (*ADH1*) promoter and human FHL3 under the conditional *MET25* promoter was constructed as follows. A *NdeI*/*SalI*-digested fragment from pGBKT7-MZF1 (18) was ligated with *SmaI*/*SalI*-digested pBridge vector (BD Biosciences). Both ends of the resulting linear DNA were blunted by T4 polymerase and subsequently ligated for self-circularization to obtain plasmid A. In contrast, pCR3.1-FHL3 antisense, which carried human FHL3 cDNA in the reverse direction in pCR3.1 vector (Invitrogen Life Technologies), was prepared by the same method as previously described for construction of pCR3.1-FHL3 (18). A *Bam*H I/*Not*I-digested fragment from pCR3.1-FHL3 antisense was ligated with *Bgl*II/*Not*I-digested pBridge vector. Adjustment of the codon frames in the yielding plasmid was achieved by digestion with *Not*I, blunting by T4 polymerase, and self-ligation. The resulting plasmid was digested with *ScaI*/*SalI* to obtain a 4.23-kb fragment. The fragment was ligated with a 4.77-kb fragment from *ScaI*/*SalI*-digested plasmid A to yield pBridge-MZF-1/FHL3. For in vitro transcription/translation of NFYC, human NFYC cDNA obtained by *SmaI*/*Xho*I digestion of pACT2-NFYC was inserted into pGADT7 vector (BD Clontech) which was digested with *Eco*RI, blunted by T4 polymerase and subsequently digested with *Xho*I to yield pGADT7-NFYC. To construct an expression plasmid of MZF-1 deletion mutant corresponding to the aa 214–485 region of human MZF-1, the MZF-1 aa 214–485 region was amplified by PCR using pGBKT7-MZF1 (18) as a template and synthetic oligonucleotides of 5′-ATGGGCGATCCCCCGGGCCCTGGCGCTA-3′ and 5′-CTACTCG GCGCTGTGGACGCGCTGGTG-3′ as primers. The amplified product was subcloned into pCR3.1 vector (Invitrogen Life Technologies). After confirming the direction and nucleotide sequence of the insert, the obtained plasmid was named pCR3.1-MZF-1 (aa 214–485).

Yeast three-hybrid assay

Matchmaker Gal4 Two-Hybrid System 3 (BD Clontech) was used according to the manufacturer's instructions. Yeast AH109 was transformed with pBridge-MZF-1/FHL3. The cells were sequentially transformed with a human lymph node cDNA library in a pACT2 vector (BD Clontech) containing a GAL4 activation domain (AD) and an hemagglutinin (HA) tag. Cotransformed cells were allowed to grow on a minimal synthetic dropout medium lacking tryptophan and leucine (SD-Trp/-Leu), because pBridge carried a *TRP1* gene and pACT2 carried a *LEU2* gene. FHL3 was only expressed in the cells cultured on the medium without methionine. Protein interaction in the cells was detected by expression of three reporter genes (*HIS3*, *ADE2*, and *MEL1*) under the control of distinct GAL4 upstream activating sequences and TATA boxes to reduce false positives. After selecting the clones expressing HIS3 on SD-Trp/-Leu/-His/-Met plates, growing colonies were transferred onto SD-Trp/-Leu/-His/-Met/-Ade(adenine) plates containing X-α-Gal to select those expressing the other reporter genes of *ADE2* and *MEL1*. X-α-Gal was purchased from BD Clontech. Furthermore, to obtain proteins interacting with MZF-1 not independent of FHL3 but dependent on FHL3, the cells which grew on the medium without methionine but hardly grew on the medium including methionine were selected. pACT2 plasmids carrying cDNA inserts were rescued from the selected clones and their nucleotide sequences were determined. The interaction among MZF-1, FHL3, and the candidate protein NFYC was retested by cotransformation of AH109 cells with pBridge-MZF-1/FHL3 and pACT2-NFYC. The cells were examined for expression of *HIS3* and *ADE2* reporter genes by testing their ability to grow on -His/-Ade medium in the absence (FHL3 was expressed) and presence (FHL3 was not expressed) of methionine.

Immunoprecipitation of in vitro-translated MZF-1, FHL3, and NFY

c-Myc-tagged MZF-1 (aa 1–217), FHL3, and HA-tagged NFYC were produced by in vitro transcription/translation method with T_NT T7 Quick Coupled Transcription/Translation System (Promega) using pGBKT7-MZF1(aa 1–217) (18), pCR3.1-FHL3 (18), and pGADT7-NFYC. The products were mixed for immunoprecipitation with anti-c-Myc mAb (Santa Cruz Biotechnology) followed by immunoblotting with anti-c-Myc and anti-HA (Roche) mAbs.

Chromatin immunoprecipitation

Cells were exposed to 1% formaldehyde for 10 min to obtain cross-linked chromatins. After washing with ice-cold PBS containing 1 mM PMSF, 1 μg/ml aprotinin, and 1 μg/ml leupeptin, the cells were resuspended in ice-cold buffer A (10 mM HEPES (pH 7.9), 10 mM potassium chloride, 0.1 mM EDTA, 1 mM DTT, 1 mM PMSF, 1 μg/ml leupeptin, and 1 μg/ml aprotinin) and incubated on ice for 10 min. Then, they were solubilized with 0.5% (v/v) Nonidet P-40 for an additional 15 min. After centrifugation at 6,000 × *g* for 1 min, nuclear pellets were resuspended in buffer S (50 mM Tris (pH 8.1), 1% SDS, 10 mM EDTA, 1 mM PMSF, 1 μg/ml leupeptin, and 1 μg/ml aprotinin) and incubated on ice for 15 min. The lysates were sonicated with Biorupter (Cosmo Bio). After centrifuging at 15,000 × g for 10 min to remove debris, the supernatants were diluted 10-fold in buffer C (16.7 mM Tris (pH 8.1), 167 mM NaCl, 0.01% SDS, 1.1% Triton X-100, 1.2 mM EDTA, 1 mM PMSF, 1 μg/ml leupeptin, and 1 μg/ml aprotinin) and precleared with 80 μl of salmon sperm DNA/protein A agarose (Upstate Biotechnology) for 1 h at 4°C. The samples were then incubated with anti-NFYC, anti-HDAC1, anti-HDAC2, anti-acetylated histone H3 or anti-acetylated histone H4 Ab for 4 h at 4°C with rotation. All five Abs were rabbit polyclonal Abs, of which anti-NFYC and anti-HDAC2 Abs were purchased from Santa Cruz Biotechnology and the remaining Abs were obtained from Upstate Biotechnology. After addition of 60 μl of salmon sperm DNA/protein A agarose, the binding reactions were incubated for an additional 1 h at 4°C with rotation. The immunoprecipitated chromatins were washed sequentially with wash buffers 1, 2, 3, and 4 (1:50 mM Tris (pH 8.1), 150 mM NaCl, 0.1% SDS, 0.5% deoxycholic acid, 1% Nonidet P-40, 2: 50 mM Tris (pH 8.1), 500 mM NaCl, 0.1% SDS, 0.5% deoxycholic acid, 1% Nonidet P-40, 3: 50 mM Tris (pH 8.1), 0.25 M LiCl, 1% Nonidet P-40, 1% deoxycholic acid, 1 mM EDTA, 4: 10 mM Tris (pH 8.0), 1 mM EDTA) and eluted from beads with elution buffer (1% SDS, 50 mM $NaHCO_3$). After incubation in the elution buffer for 15 min at room temperature with rotation, supernatants were separated by centrifugation. To reverse cross-linking, the eluates were incubated at 65°C for 4 h in a buffer containing 200 mM NaCl and 1 μg of RNase A followed by treatment with 20 μg of proteinase K in 40 mM Tris (pH 6.5), 10 mM EDTA at 45°C for 1 h. DNA was recovered by phenol/chloroform extraction and ethanol precipitation. The precipitates were resuspended in sterile water and subjected to PCR analyses using synthetic oligonucleotides of 5′-CTGGAATGTTGTCAATTATATCTGAAAGG-3′ and 5′-CT GTTCTTCTTATCTTTTCAAGGATGGAC-3′ specific for the β-chain fourth intron region as primers. Primers of 5′-TGCCTAGGTCACCCAC TAATG-3′ and 5′-GTGGCCCGTGATGAAGGCTA-3′ (22) that specifically recognize the β-actin promoter sequences were used as control. A thermal cycle of 95°C for 30 s, 55°C for 30 s, and 72°C for 1 min was repeated 33 times. Sizes of the fragments amplified by the β-chain intronic region-specific and β-actin promoter region-specific primers were 99 and 160 bp, respectively.

Transfection of the cells

KU812 cells were suspended in the medium containing 20% FBS at the concentration of 5 × 10^6 cells/500 μl. The cells were transfected with 5 μg

of pCR3.1-MZF-1(aa 214–485) or an empty vector pCR3.1-self (17) as control by electroporation at 300 V, 950 μF using Gene Pulser II (Bio-Rad) and cultured for 16 h. To select transfected cells, the cells were then cultured with 400 μg/ml G418 until they were subjected for the assay.

Quantitation of FcεRI β-chain mRNA levels by real-time RT-PCR

Total RNA was isolated from cells cultured in the presence or absence of 10 ng/ml GM-CSF for 1–10 days with TRIzol reagent (Invitrogen Life Technologies) and was reverse transcribed with TaqMan Reverse Transcription Reagents (Applied Biosystems) using an oligo$(dT)_{16}$ primer. Quantitative PCR was performed with TaqMan Universal PCR Master Mix without UNG AmpErase (Applied Biosystems) using human FcεRI β-chain-specific and human β-actin-specific primers and fluorescent probes (Applied Biosystems). Reactions were conducted with the conditions of 95°C for 10 min followed by 50 cycles of 95°C for 15 s and 60°C for 1 min by ABI PRISM 7700 Sequence Detection System (Applied Biosystems). Relative expression levels of β-chain and β-actin were calculated respectively from the standard curve using a dilution series of template RNA. The expression levels of β-chain were normalized by those of β-actin.

Results

NFY forms a complex with MZF-1/FHL3

We at first tried to identify constituents of the large nuclear complex which contained MZF-1/FHL3 and suppressed human FcεRI β-chain gene expression through the element in the fourth intron. A human cDNA library was screened for proteins forming a ternary complex with MZF-1 and FHL3 by yeast three-hybrid assay (Fig. 1, *A* and *B*). An expression plasmid which carried MZF-1 cDNA fused to GAL4BD under the constitutive ADH1 promoter (P_{ADH1}) and FHL3 cDNA under the conditional Met25 promoter (P_{Met25}) repressed with methionine was constructed. Full-length MZF-1 fused to GAL4BD did not autonomously activate the reporter (18). The construct was introduced into a yeast AH109 strain with a human cDNA library-GAL4AD fusion expression plasmid to search proteins forming a ternary complex with MZF-1/FHL3. As represented in Fig. 1*C*, we screened 2.6×10^6 cDNA clones and obtained 188 positive clones expressing all three reporter genes of *HIS3*, *ADE2*, and *MEL1*. To distinguish the clones which encoded proteins interacting with MZF-1 in an FHL3-dependent manner from those encoded proteins directly binding MZF-1 independent of FHL3, the cells which grew on the medium without methionine, but hardly grew on the medium including methionine, were selected. Of 11 clones obtained, 10 clones encoded three different proteins and the remaining clone did not have a cDNA insert in frame.

The C subunit of the transcription factor NFY was one of the three identified proteins. To verify that NFYC interacts with MZF-1 through FHL3 to form a ternary complex, yeast AH109 cells were cotransformed with constructs carrying P_{ADH1}-BD-MZF-1/P_{Met25}-FHL3 and P_{ADH1}-AD-NFYC, respectively. Growth of the transformed cells was examined on -His/-Ade medium to test the expression of two reporter genes of *HIS3* and *ADE2*. The transformed cells grew on the -His/-Ade medium in the absence of methionine (FHL3 was expressed) but did not grew in the presence of methionine (FHL3 was not expressed) (Fig. 2*A*). To further confirm the interaction, c-Myc-tagged BD-MZF-1, FHL3, and HA-tagged AD-NFYC were produced by in vitro transcription/translation method. Their mixtures were immunoprecipitated with anti-c-Myc tag Ab. Because the full-length MZF-1 fused to BD was not expressed efficiently by in vitro transcription/translation, the aa 1–217 region of MZF-1 which could bind FHL3 (18) was used. BD-MZF-1 and AD-NFYC were coimmunoprecipitated in the presence of FHL3 but were not in the absence of FHL3 (Fig. 2*B*). Both of the results from Fig. 2 demonstrated that NFYC interacted with MZF-1 through FHL3 and formed a ternary complex,

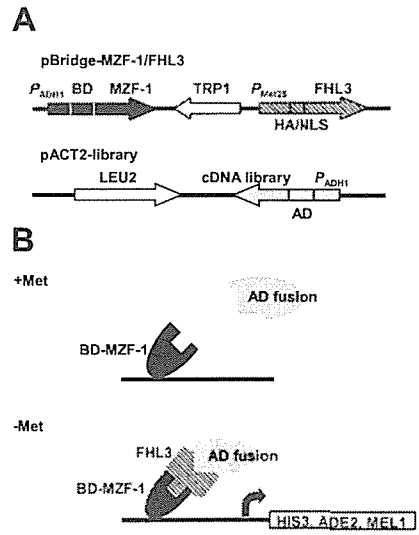

C

screened	HIS3	ADE2, MEL1	Growth -Met > +Met
2.6×10^6	1259	188	11

FIGURE 1. Screening of a human cDNA library by yeast three-hybrid assay. *A*, Structures of expression plasmids used for the yeast three-hybrid screen are shown. MZF-1 cDNA fused to GAL4BD and FHL3 cDNA are inserted into pBridge vector under the constitutive *ADH1* promoter and the conditional *MET25* promoter, respectively (pBridge-MZF-1/FHL3). A human cDNA library is fused to GAL4AD in pACT2 vector (pACT2-library). *B*, In the three-hybrid assay, FHL3 is expressed only in the absence of methionine. If a protein encoded by pACT2-library forms a ternary complex with FHL3 and MZF-1 as indicated in the figure, expression of reporter genes (*HIS3*, *ADE2*, *MEL1*) is activated. *C*, Yeast AH109 was sequentially transformed with pBridge-MZF-1/FHL3 and pACT2-library. After selecting the clones expressing HIS3 reporter on -Trp/-Leu/-His/-Met medium, growing colonies were then tested for expression of ADE2 and MEL1 reporters on -Trp/-Leu/-His/-Met/-Ade medium containing X-α-Gal. To obtain the clones which encoded proteins interacting with MZF-1 in an FHL3-dependent manner, the cells expressing all three reporter genes were further selected, based on their poor growth on -Trp/-Leu/-His/-Ade medium containing methionine.

indicating that NFYC was a candidate constituting the large regulatory complex, which repressed human β-chain gene expression through the element in the fourth intron, with MZF-1 and FHL3 in the nucleus.

NFY and HDAC interact with the fourth intron region of the human FcεRI β-chain gene

We next analyzed whether NFYC was actually involved in the transcriptional regulation of the human FcεRI β-chain gene. To examine whether NFYC interacts with the fourth intron region of the β-chain gene in the context of chromatin in vivo, chromatin immunoprecipitation (ChIP) assays of the endogenous β-chain gene in the human mast cell line HMC-1 were conducted. As shown in Fig. 3*A*, the fourth intron region of the β-chain gene corresponding to nt 4133–4231 (represented nucleotide numbers begin at the transcription start site as position +1) which included the MZF-1-binding element was amplified from chromatins immunoprecipitated with anti-NFYC Ab but scarcely amplified from those immunoprecipitated with control rabbit IgG. In contrast, the β-actin promoter region was amplified only at a low level from both chromatins immunoprecipitated with anti-NFYC Ab and control IgG. Relative band intensities to those from the input fraction

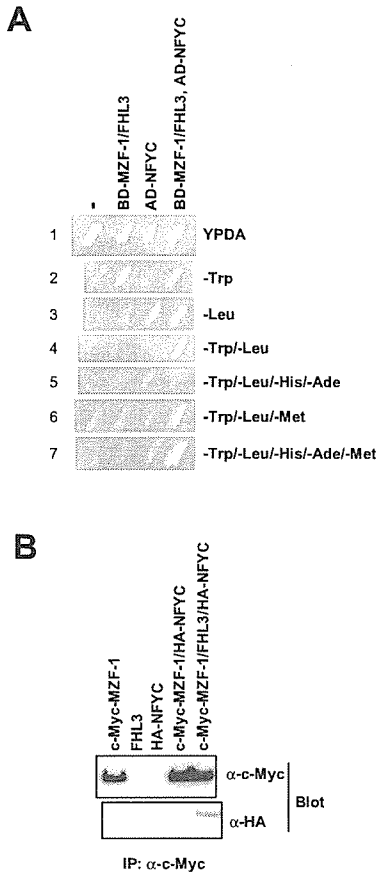

FIGURE 2. NFYC interacts with MZF-1 through FHL3. *A*, Yeast AH109 was cotransformed with pBridge-MZF-1/FHL3 and pACT2-NFYC to test interaction among MZF-1, FHL3, and NFYC. The cells were examined for expression of *HIS3* and *ADE2* reporter genes by testing their ability to grow on -Trp/-Leu/-His/-Ade medium in the absence (FHL3 was expressed, *panel 7*) and presence (FHL3 was not expressed, *panel 5*) of methionine. *B*, c-Myc-tagged MZF-1, FHL3, and HA-tagged NFYC were prepared by in vitro transcription/translation. These proteins were mixed with the indicated combination, immunoprecipitated with anti-c-Myc mAb, and subsequently blotted with anti-c-Myc and anti-HA mAbs.

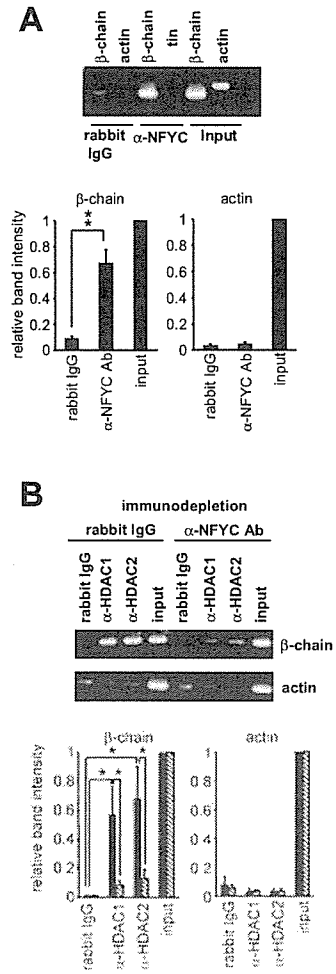

FIGURE 3. NFYC and HDAC interact with the fourth intron region of the β-chain gene. *A*, ChIP assays of the endogenous β-chain gene in HMC-1 cells were performed using anti-NFYC Ab. Rabbit IgG was used as control. The fourth intron region nt 4133/4231 of the β-chain gene and the promoter region of the β-actin gene as control were amplified by PCR from the immunoprecipitated chromatins. The lanes of "input" represent the results of PCR using diluted fractions of nonimmunoprecipitated chromatins as templates to quantitate the amount of DNA present in each sample before immunoprecipitation. Amplified fragments of the β-chain intronic region and the β-actin promoter region were 99 and 160 bp, respectively. *B*, ChIP assays of the endogenous β-chain gene in HMC-1 cells were similarly performed using anti-HDAC1 and anti-HDAC2 Abs. The chromatins were immunodepleted with anti-NFYC Ab or control rabbit IgG before immunoprecipitation with anti-HDAC Abs. Data shown are representative of four (*A*) or three (*B*) independent experiments. Relative band intensities to those from input fractions are expressed in the graphs as means ± SD of the four (*A*) or three (*B*) experiments. In *B*, ■ and ▨ express the results of immunodepletion experiments with control IgG and anti-NFYC Ab, respectively. Statistically significant differences with the two-tailed Student *t* test are indicated by asterisks (**, $p < 0.005$ and *, $p < 0.05$).

were represented in the graphs. The band intensity of β-chain intron region amplified from the fraction immunoprecipitated with anti-NFYC was significantly higher than that from the fraction immunoprecipitated with control IgG ($p < 0.005$), but the band intensities of the β-actin promoter region from the fractions immunoprecipitated with anti-NFYC Ab and control IgG were not significantly different. These results indicated that NFYC specifically interacted with the β-chain gene region including the element in the fourth intron.

NFY consists of A, B, and C subunits (23), of which the A subunit has been reported to bind HDACs (24). Therefore, we analyzed the interaction between HDACs and the intronic region of the β-chain gene by ChIP assays using anti-HDAC1 and anti-HDAC2 Abs (Fig. 3*B*). The β-chain intron region was significantly, more highly amplified from chromatins immunoprecipitated with anti-HDAC1 or anti-HDAC2 Ab than from those immunoprecipitated with rabbit IgG as control ($p < 0.05$). In contrast, amplification of the β-actin promoter region from chromatins immunoprecipitated with anti-HDAC Abs was as low as that from chromatins immunoprecipitated with control IgG. Therefore, it was demonstrated that HDAC1 and HDAC2 interacted with the β-chain gene region including the element in the fourth intron. Furthermore, pretreatment with anti-NFYC Ab resulted in remarkable decrease of amplification of the β-chain intron region ($p < 0.05$, vs control IgG pretreatment), indicating that NFYC was actually required for the recruitment of HDACs to the β-chain gene.

The experiments of Fig. 3 revealed that NFY and HDACs interacted with the β-chain gene region including the element in the fourth intron in the context of chromatin in vivo. The results suggested a possibility that HDACs, which were recruited to the β-chain gene through the NFY/FHL3/MZF-1 complex, deacetylated histones to repress the transcription. It was also suggested

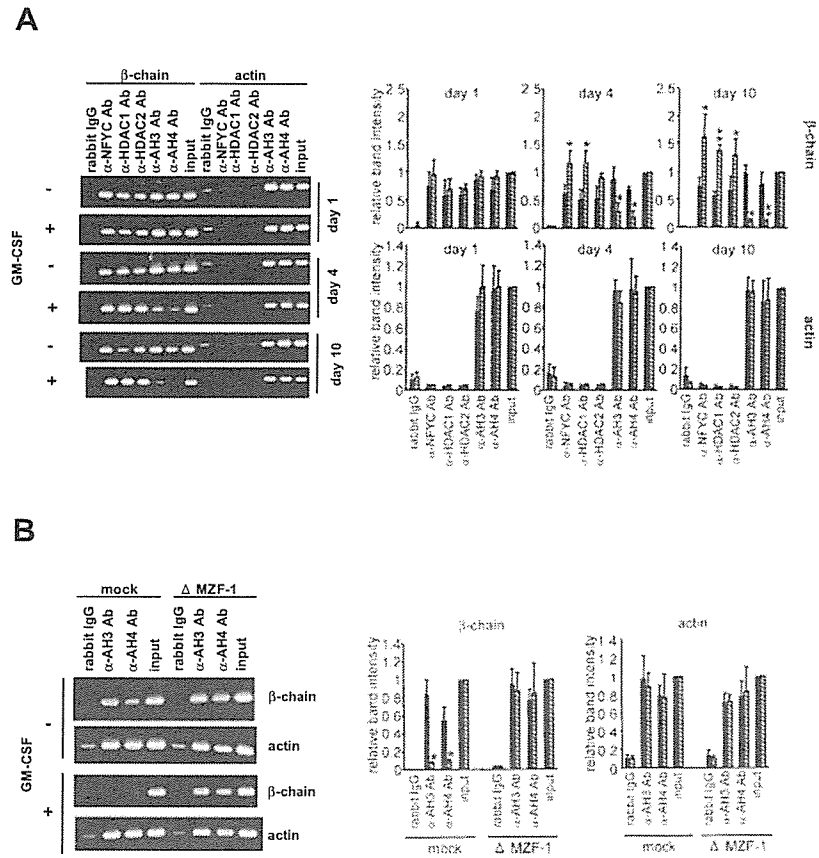

FIGURE 4. GM-CSF decreases acetylation of histones interacting with the fourth intron region of the β-chain gene in an MZF1/FHL3-dependent manner. *A*, HMC-1 cells cultured with or without 10 ng/ml GM-CSF for 1, 4, and 10 days were subjected to ChIP assays. The chromatins immunoprecipitated with anti-NFYC, anti-HDAC1, anti-HDAC2, anti-acetylated histone H3 (α-AH3), and anti-acetylated histone H4 (α-AH4) Abs were amplified by PCR using primers specific for the intronic element of the β-chain gene and the β-actin promoter as control. Rabbit IgG was used as control. The lanes of "input" represent the results of PCR using diluted fractions of nonimmunoprecipitated chromatins as templates. *B*, An expression plasmid of MZF-1 deletion mutant (ΔMZF-1) which lacked the region binding FHL3 or an empty vector as control were respectively introduced into KU812 cells. After culturing the transfected cells with or without 10 ng/ml GM-CSF for 7 days, ChIP assays using anti-acetylated histone H3 and anti-acetylated histone H4 Abs were performed. Data shown are representative of three independent experiments. Relative band intensities to those from input fractions are expressed in the graphs as means ± SD of the three experiments. ■ and ▨ represent the results of cells cultured in the absence and presence of GM-CSF, respectively. Results of statistical analysis with the two-tailed Student *t* test between GM-CSF-treated and nontreated cells are as follows: *, $p < 0.05$ and **, $p < 0.005$.

that the transcriptional repression of the β-chain gene was promoted by GM-CSF which induced up-regulation of MZF-1 (19) and nuclear translocation of FHL3 (18), because it was predicted that recruitment of HDACs to the β-chain gene was facilitated by increased formation of the large regulatory complex containing MZF-1 and FHL3 in the nucleus.

GM-CSF decreases histone acetylation of the human FcεRI β-chain gene and suppresses β-chain gene expression

To determine whether HDAC activities were involved in the transcriptional repression of the β-chain gene through the element in the fourth intron, acetylation levels of histones were compared between the cells cultured in the presence and absence of GM-CSF for 1, 4, and 10 days. ChIP assays were conducted using anti-acetylated histone H3 and anti-acetylated histone H4 Abs to analyze whether the intronic region of the β-chain gene associates with acetylated histones in HMC-1 cells (Fig. 4*A*). Amplification of the β-chain fourth intron region from both of the chromatins immunoprecipitated with anti-acetylated histone H3 and anti-acetylated histone H4 Abs was not changed by GM-CSF at day 1 but significantly decreased by GM-CSF at days 4 and 10 ($p < 0.05$ vs without GM-CSF). The amounts of the amplified products of the β-actin promoter were not affected by GM-CSF. It was thus demonstrated that acetylation of histones interacted with the fourth intron region of the β-chain gene was decreased in HMC-1 cells cultured with GM-CSF for 4–10 days. Parallel to the decrease of histone acetylation, interaction of NFYC and HDACs with the β-chain gene was increased at day 4 and more remarkably increased at day 10, suggesting that the decreased histone acetylation was mediated by HDACs which were recruited to the β-chain gene through NFY.

Table I. *Effect of GM-CSF on FcεRI β-chain gene expression*[a]

	Day 0	Day 1	Day 4	Day 10
−	1.00	1.06 ± 0.0600	1.06 ± 0.160	1.11 ± 0.153
GM-CSF +		1.56 ± 0.170[b]	0.697 ± 0.115[b]	0.289 ± 0.0424[c]

[a] HMC-1 cells were cultured with or without 10 ng/ml GM-CSF for the indicated periods. After collecting and washing the cells, total RNA was prepared to quantify mRNAs of FcεRI β-chain and β-actin by real-time RT-PCR. The amounts of β-chain mRNA corrected with the amounts of β-actin mRNA are represented as relative values to those at day 0. Values are expressed as means ± SD of three independent experiments.

[b] Significantly different from the value in the absence of GM-CSF ($p < 0.05$).

[c] Significantly different from the value in the absence of GM-CSF ($p < 0.01$).

In the previous report, we revealed that MZF-1 bound FHL3 through four zinc finger motifs at its N-terminal (18). An expression plasmid of the MZF-1 deletion mutant which lacked this FHL3-interacting region was constructed and introduced into a human basophilic leukemia cell line KU812 which was known to express mast cell-specific molecules, because HMC-1 cells gave very low transfection efficiency. By similar ChIP assays using anti-acetylated histone H3 and anti-acetylated histone H4 Abs, it was shown that association between the intronic region of the β-chain gene and acetylated histones was not decreased in the cells cultured with GM-CSF for 7 days when the MZF-1 deletion mutant was overexpressed, while the association was significantly decreased in the mock-transfected cells by GM-CSF (Fig. 4*B*). The β-chain mRNA expression was decreased to approximately one-half in KU812 cells cultured with GM-CSF for 7 days (data not shown). These results indicated that the decrease of histone acetylation in the presence of GM-CSF was mediated through the regulatory complex including MZF-1/FHL3/NFY.

We further analyzed whether FcεRI β-chain expression was repressed in HMC-1 cells cultured in the presence of GM-CSF by real-time RT-PCR. As represented in Table I, the cells cultured

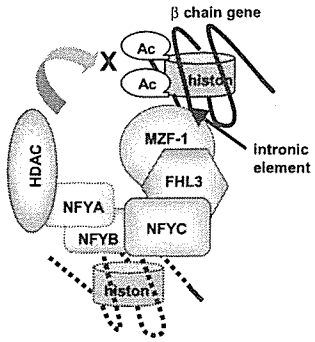

FIGURE 5. A schematic drawing of a model for histone deacetylation-mediated regulation of β-chain gene expression. Histone deacetylation-mediated regulatory mechanisms of β-chain gene expression suggested by our study are described schematically. Ac, acetyl group.

with GM-CSF for 4 and 10 days expressed significantly smaller amounts of β-chain mRNA compared with the cells cultured without GM-CSF ($p < 0.05$ at day 4 and $p < 0.01$ at day 10), although they expressed a slightly but reproducibly increased level of β-chain mRNA at day 1 in the presence of GM-CSF ($p < 0.05$ vs without GM-CSF). These results showed that sustained exposure to GM-CSF, which decreased acetylation of histones interacting with the β-chain gene, suppressed β-chain gene expression.

Collectively, it was suggested that the repression of β-chain gene expression in the presence of GM-CSF was dependent on deacetylation of histones by HDACs which were recruited to the β-chain gene through the MZF-1/FHL3/NFY complex.

Discussion

We revealed that FcεRI β-chain gene expression was repressed in the cells cultured with GM-CSF and this transcriptional repression was correlated with histone deacetylation of the β-chain gene. Fig. 5 describes mechanisms for the HDAC-mediated transcriptional repression which are suggested from our study. Increased histone deacetylation of the β-chain gene in the presence of GM-CSF was thought to be dependent on enhanced formation of the HDAC/NFY/FHL3/MZF-1 complex in the nucleus, because expression of MZF-1 and nuclear translocation of FHL3 were induced by GM-CSF (18). Although the expression of NFY was not affected by GM-CSF (data not shown), there still remains a possibility that expression or subcellular localization of unidentified factors in the large regulatory complex including HDAC/NFY/FHL3/MZF-1 was influenced by GM-CSF.

The cell surface expression of FcεRI has been reported to be suppressed by GM-CSF in HMC-1 cells where α-chain mRNA was decreased (20, 21). Because our study showed that β-chain expression was also repressed, suppression of both α and β-chain gene expression was thought to contribute to the decrease of FcεRI expression in the cells cultured with GM-CSF. GM-CSF is a hemopoietic cytokine which promotes differentiation and proliferation of myeloid cells. GM-CSF is also known to inhibit terminal differentiation of mast cells. These observations suggest that GM-CSF plays a particular role in myeloid cell differentiation by repressing the expression of FcεRI in the cells differentiating into eosinophils, neutrophils, or monocytes which express low or undetectable levels of FcεRI in their resting states. In addition to the effects on hemopoietic cell differentiation, GM-CSF plays a key role in peripheral inflammatory processes by enhancing functional activities of mature myeloid effector cells. Therefore, the regulatory mechanisms of FcεRI expression induced by GM-CSF will also contribute to the control of FcεRI-mediated functions of peripheral cells under specific circumstances.

Interestingly, the amount of β-chain mRNA was once slightly increased before it was significantly decreased by GM-CSF (Table I). In the time course analyses in Fig. 4*A* and Table I, while the expression of β-chain gene expression was decreased at days 4–10 parallel to the increased association of NFYC and HDACs with the β-chain gene, neither significant difference of NFYC or HDAC interaction nor that of histone acetylation was observed between days 0 and 1. Therefore, it was thought that the slight increase of β-chain gene expression observed at day 1 was not due to decreased association of NFY/HDAC with the fourth intron region of the β-chain gene. However, we could not neglect the possibility that the change of NFY or HDAC interaction was small and not sufficient to be detected by ChIP assays. Although it is not clear what this phenomenon means at present, it may possibly reflect bidirectional regulation through the MZF-1-binding element, because we found that MZF-1 could activate β-chain gene transcription with a different cofactor when the cofactor was overexpressed (K. Takahashi, N. Hayashi, and C. Ra, manuscript in preparation). The MZF-1-binding element in the fourth intron is thought to repress and activate β-chain gene transcription depending on cofactor availability. The equilibrium will markedly incline to the transcriptional repression in the presence of GM-CSF, but nuclear translocation of FHL3 which was observed 24 h after the addition of GM-CSF (18) may not be sufficient to shift the equilibrium, judging from the fact that β-chain mRNA was temporally increased before it was significantly decreased by GM-CSF.

This is the first report that revealed the binding between FHL3 and NFY. FHL3 is a member of four-and-a-half LIM only protein (FHL) family including FHL1, FHL2, FHL3, FHL4, and ACT (25–30). They only contain a single N-terminal half-LIM domain followed by four sequential LIM domains, belonging to a subset of the LIM protein superfamily which possesses cysteine-rich double zinc finger motifs called LIM. FHL proteins are expressed in a cell- and tissue-specific manner and participate in various cellular processes by interacting with actin cytoskeleton in the cytoplasm and with transcriptional machinery in the nucleus. These studies suggest that FHL proteins function as adaptors or scaffolds to support the assembly of multimeric protein complex. Although there are several reports that FHL family proteins act as coactivators or corepressors of transcription factors (31–34), precise mechanisms by which FHL proteins mediate the protein interaction and exert their functions as transcriptional cofactors remain to be elucidated. Our study presented just an example that FHL3 was involved in the transcriptional regulation by functioning as an adaptor molecule which linked the HDAC-containing protein complex with a transcription factor/DNA complex.

NFY is a heterotrimeric transcription factor which is known to bind CCAAT motifs in the proximal promoter of a wide variety of genes and activate transcription, particularly in TATA-less genes. Among the three subunits constituting NFY, A and B-subunits have been reported to bind HDAC and p300/CBP, respectively (24, 35). These reports indicate that NFY can directly interact with both histone acetyl transferase and HDAC, which are known to act as a transcriptional coactivator and corepressor, respectively. It has been actually reported that NFY functions not only as an activator but also as a repressor depending on promoter contexts and cell types (36–39). Interestingly, NFY functions as a repressor by binding a DNA sequence different from its consensus-binding motif CCAAT (36), suggesting that NFY binds different DNA sequences through its different domains. It is thought that NFY changes its conformation by binding to the different DNA sequences via its different domains, which allows NFY to specifically bind histone acetyl transferase or HDAC. There is no typical CCAAT-binding motif in the human β-chain gene, but NFY may

bind to a noncanonical-binding motif in the β-chain gene region apart from the element in the fourth intron and interact with the FHL3/MZF-1 complex. In that case, deacetylation of histones may not be limited in the region close to the element in the fourth intron but may spread out to a more broad region of the β-chain gene.

In this study, we revealed the histone deacetylation-mediated mechanisms for transcriptional regulation of the human FcεRI β-chain gene through the element in the fourth intron. The concrete and specific information about the molecules and their interactions which participate in the regulation of β-chain gene expression like this will contribute to applications to the development of therapeutic and prophylactic drugs for allergy. More detailed study including the analyses on regulatory mechanisms through other elements of the β-chain gene will reveal the entire regulatory mechanisms of FcεRI β-chain gene expression.

Acknowledgments

We thank the members of Division of Molecular Cell Immunology and Allergology for helpful discussions.

Disclosures

The authors have no financial conflict of interest.

References

1. Gounni, A. S., B. Lamkhioued, K. Ochiai, Y. Tanaka, E. Delaporte, A. Capron, J. P. Kinet, and M. Capron. 1994. High-affinity IgE receptor on eosinophils is involved in defense against parasites. *Nature* 367: 183–186.
2. Maurer, D., E. Fiebiger, B. Reininger, B. Woff-Winski, M. H. Jouvin, O. Kilgus, J. P. Kinet, and G. Stingl. 1994. Expression of functional high affinity immunoglobulin E receptors (FcεRI) on monocytes of atopic individuals. *J. Exp. Med.* 179: 745–750.
3. Bieber, T., H. de la Salle, A. Wollenberg, J. Hakimi, R. Chizzonite, J. Ring, D. Hanau, and C. de la Salle. 1992. Human epidermal Langerhans cells express the high affinity receptor for immunoglobulin E (FcεRI). *J. Exp. Med.* 175: 1285–1290.
4. Wang, B., A. Rieger, O. Kilgus, K. Ochiai, D. Maurer, D. Fodinger, J. P. Kinet, and G. Stingl. 1992. Epidermal Langerhans cells from normal human skin bind monomeric IgE via FcεRI. *J. Exp. Med.* 175: 1353–1365.
5. Joseph, M., A. S. Gounni, J. P. Kusnierz, H. Vorng, M. Sarfati, J. P. Kinet, A. B. Tonnel, A. Capron, and M. Capron. 1997. Expression and functions of the high-affinity IgE receptor on human platelets and megakaryocyte precursors. *Eur. J. Immunol.* 27: 2212–2218.
6. Hasegawa, S., R. Pawankar, K. Suzuki, T. Nakahata, S. Furukawa, K. Okumura, and C. Ra. 1999. Functional expression of the high affinity receptor for IgE (FcεRI) in human platelets and its' intracellular expression in human megakaryocytes. *Blood* 93: 2543–2551.
7. Gounni, A. S., B. Lamkhioued, L. Koussih, C. Ra, P. M. Renzi, and Q. Hamid. 2001. Human neutrophils express the high-affinity receptor for immunoglobulin E (FcεRI): role in asthma. *FASEB J.* 15: 940–949.
8. Miller, L., U. Blank, H. Metzer, and J. P. Kinet. 1989. Expression of high-affinity binding of human immunoglobulin E by transfected cells. *Science* 244: 334–337.
9. Lin, S., C. Cicala, A. M. Scharenberg, and J. P. Kinet. 1996. The FcεRI β subunit functions as an amplifier of FcεRI γ-mediated cell activation signals. *Cell* 85: 985–995.
10. Dombrowicz, D., S. Lin, V. Flamand, A. T. Brini, B. H. Koller, and J. P. Kinet. 1998. Allergy-associated FcεRβ is a molecular amplifier of IgE- and IgG-mediated in vivo responses. *Immunity* 8: 517–529.
11. Donnadieu, E., M. H. Jouvin, and J. P. Kinet. 2000. A second amplifier function for the allergy-associated FcεRI β subunit. *Immunity* 12: 515–523.
12. Furumoto, Y., S. Nunomura, T. Terada, J. Rivera, and C. Ra. 2004. The FcεRIβ immunoreceptor tyrosine-based activation motif exerts inhibitory control on MAPK and IκB kinase phosphorylation and mast cell cytokine production. *J. Biol. Chem.* 279: 49177–49187.
13. Donnadieu, E., M. H. Jouvin, S. Rana, M. F. Moffatt, E. H. Mockford, W. O. Cookson, and J. P. Kinet. 2003. Competing functions encoded in the allergy-associated FcεRIβ gene. *Immunity* 18: 665–674.
14. Kurosaki, T., I. Gander, U. Wirthmueller, and J. V. Ravetch. 1992. The β subunit of the FcεRI is associated with the FcγRIII on mast cells. *J. Exp. Med.* 175: 447–451.
15. Kuster, H., L. Zhang, A. T. Brini, D. W. MacGlashan, and J. P. Kinet. 1992. The gene and cDNA for the human high affinity immunoglobulin E receptor β chain and expression of the complete human receptor. *J. Biol. Chem.* 267: 12782–12787.
16. Akizawa, Y., C. Nishiyama, M. Hasegawa, K. Maeda, T. Nakahata, K. Okumura, C. Ra, and H. Ogawa. 2003. Regulation of human FcεRI β chain gene expression by Oct-1. *Int. Immunol.* 15: 549–556.
17. Takahashi, K., C. Nishiyama, M. Hasegawa, Y. Akizawa, and C. Ra. 2003. Regulation of the human high affinity IgE receptor β-chain gene expression via an intronic element. *J. Immunol.* 171: 2478–2484.
18. Takahashi, K., C. Matsumoto, and C. Ra. 2005. FHL3 negatively regulates human high-affinity IgE receptor β-chain gene expression by acting as a transcriptional co-repressor of MZF-1. *Biochem. J.* 385: 191–200.
19. Hui, P., X. Guo, and P. G. Bradford. 1995. Isolation and functional characterization of the human gene encoding the myeloid zinc finger protein MZF-1. *Biochemistry* 34: 16493–16502.
20. Welker, P., J. Grabbe, T. Zuberbier, A. Grützkau, and B. M. Henz. 2001. GM-CSF downmodulates c-*kit*, FcεRIα and GM-CSF receptor expression as well as histamine and tryptase levels in cultured human mast cells. *Arch. Dermatol. Res.* 293: 249–258.
21. Welker, P., J. Grabbe, T. Zuberbier, and B. M. Henz. 1997. GM-CSF downregulates expression of tryptase, FcεRI and histamine in HMC-1 cells. *Int. Arch. Allergy Immunol.* 113: 284–286.
22. Ponte, P., S. Y. Ng, J. Engel, P. Gunning, and L. Kedes. 1994. Evolutionary conservation in the untranslated regions of actin mRNAs: DNA sequence of a human β-actin cDNA. *Nucleic Acids Res.* 12: 1687–1696.
23. Maity, S. N., and B. De Crombrugghe. 1996. Purification, characterization, and role of CCAAT-binding factor in transcription. *Methods Enzymol.* 273: 217–232.
24. Peng, Y., and N. Jahroudi. 2003. The NFY transcription factor inhibits von Willebrand factor promoter activation in non-endothelial cells through recruitment of histone deacetylases. *J. Biol. Chem.* 278: 8385–8394.
25. Greene, W. K., E. Baker, T. H. Rabbitts, and U. R. Kees. 1999. Genomic structure, tissue expression and chromosomal location of the LIM-only gene, SLIM1. *Gene* 232: 203–207.
26. Chan, K. K., S. K. Tsui, S. M. Lee, S. C. Luk, C. C. Liew, K. P. Fung, M. M. Waye, and C. Y. Lee. 1998. Molecular cloning and characterization of FHL2, a novel LIM domain protein preferentially expressed in human. *Gene* 210: 345–350.
27. Morgan, M. J., and A. J. Madgwick. 1996. Slim defines a novel family of LIM-proteins expressed in skeletal muscle. *Biochem. Biophys. Res. Commun.* 225: 632–638.
28. Taniguchi, Y., T. Furukawa, T. Tun, H. Han, and T. Honjo. 1998. LIM protein KyoT2 negatively regulates transcription by association with the RBP-J DNA-binding protein. *Mol. Cell. Biol.* 18: 644–654.
29. Morgan, M. J., and A. J. Madgwick. 1999. The fourth member of the FHL family of LIM proteins is expressed exclusively in the testis. *Biochem. Biophys. Res. Commun.* 255: 251–255.
30. Morgan, M. J., A. J. Madgwick, B. Charleston, J. M. Pell, and P. T. Loughna. 1995. The developmental regulation of a novel muscle LIM-protein. *Biochem. Biophys. Res. Commun.* 212: 840–846.
31. Turner, J., H. Nicholas, D. Bishop, J. M. Matthews, and M. Crossley. 2003. The LIM protein FHL3 binds Kruppel-like factor/Kruppel-like factor 3 and its co-repressor C-terminal-binding protein 2. *J. Biol. Chem.* 278: 12786–12795.
32. Fimia, G. M., D. De Cesare, and P. Sassone-Corsi. 2000. A family of LIM-only transcriptional coactivators: tissue-specific expression and selective activation of CREB and CREM. *Mol. Cell. Biol.* 20: 8613–8622.
33. Fimia, G. M., D. De Cesare, and P. Sassone-Corsi. 1999. CBP-independent activation of CREM and CREB by the LIM-only protein ACT. *Nature* 398: 165–169.
34. Muller, J. M., U. Isele, E. Metzger, A. Rempel, M. Moser, A. Pscherer, T. Breyer, C. Holubarsch, R. Buettner, and R. Schule. 2000. FHL2, a novel tissue-specific coactivator of the androgen receptor. *EMBO J.* 19: 359–369.
35. Faniello, M. C., M. A. Bevilacqua, G. Condorelli, B. de Crombrugghe, S. N. Maity, E. Avvedimento, F. Cimino, and F. Costanzo. 1999. The B subunit of the CAAT-binding factor NFY binds the central segment of the co-activator p300. *J. Biol. Chem.* 274: 7623–7626.
36. Peng, Y., and N. Jahroudi. 2002. The NFY transcription factor functions as a repressor and activator of the von Willebrand factor promoter. *Blood* 99: 2408–2417.
37. Zhou, D., S. Masri, J. J. Ye, and S. Chen. 2005. Transcriptional regulation of the mouse PNRC2 promoter by the nuclear factor Y (NFY) and E2F1. *Gene* 361: 89–100.
38. Nicolas, M., V. Noe, and C. J. Ciudad. 2003. Transcriptional regulation of the human Sp1 gene promoter by the specificity protein (Sp) family members nuclear factor Y (NF-Y) and E2F. *Biochem. J.* 371: 265–275.
39. Radomska, H. S., A. B. Satterthwaite, N. Taranenko, S. Narravula, D. S. Krause, and D. G. Tenen. 1999. A nuclear factor Y (NFY) site positively regulates the human CD34 stem cell gene. *Blood* 94: 3772–3780.

APPLIED AND ENVIRONMENTAL MICROBIOLOGY, Sept. 2006, p. 6271–6276 Vol. 72, No. 9
0099-2240/06/$08.00+0 doi:10.1128/AEM.00477-06

Increase in Terminal Restriction Fragments of *Bacteroidetes*-Derived 16S rRNA Genes after Administration of Short-Chain Fructooligosaccharides

Yusuke Nakanishi,[1]† Koichiro Murashima,[2]*† Hiroki Ohara,[2] Takahisa Suzuki,[3] Hidenori Hayashi,[4] Mitsuo Sakamoto,[4] Tomoyuki Fukasawa,[2] Hidetoshi Kubota,[2] Akira Hosono,[1] Toshiaki Kono,[2] Shuichi Kaminogawa,[1] and Yoshimi Benno[4]

Department of Food Science and Technology, College of Bioresource Sciences, Nihon University, 1866 Kameino, Fujisawa, Kanagawa 252-8510,[1] Food and Health R&D Laboratories, Meiji Seika Kaisha, Ltd., 5-3-1 Chiyoda, Sakado, Saimata 350-0289,[2] Pharmaceutical Research Department, Meiji Seika Kaisha, Ltd., 760 Morooka, Kohoku-Ku, Yokohama, Kanagawa 222-8567,[3] and Microbe Division, Japan Collection of Microorganisms, RIKEN BioResource Center, 2-1 Hirosawa, Wako, Saitama 351-0198,[4] Japan

Received 27 February 2006/Accepted 22 June 2006

It is well known that short chain fructooligosaccharides (scFOS) modify intestinal microbiota in animals as well as in humans. Since most murine intestinal bacteria are still uncultured, it is difficult for a culturing method to detect changes in intestinal microbiota after scFOS administration in a mouse model. In this study, we sought markers of positive change in murine intestinal microbiota after scFOS administration using terminal restriction fragment length polymorphism (T-RFLP) analysis, which is a culture-independent method. The T-RFLP profiles showed that six terminal restriction fragments (T-RFs) were significantly increased after scFOS administration. Phylogenetic analysis of the 16S rRNA partial gene sequences of murine fecal bacteria suggested that four of six T-RFs that increased after scFOS administration were derived from the 16S rRNA genes of the class *Bacteroidetes*. Preliminary quantification of *Bacteroidetes* by real-time PCR suggests that the 16S rRNA genes derived from *Bacteroidetes* were increased by scFOS administration. Therefore, the T-RFs derived from *Bacteroidetes* are good markers of change of murine intestinal microbiota after scFOS administration.

Short-chain fructooligosaccharide (scFOS) is one of the popular prebiotics (4). The scFOS is a mixture of oligosaccharides consisting of a glucose (G) unit linked to fructose (F) units (n = 2 to 4) (6). The scFOS arrives at the gastrointestinal tract without digestion and is used as a carbon source by intestinal bacteria (14). Consequently, the composition of intestinal microbiota is changed by scFOS administration (5).

It is known that scFOS has several physiological effects on humans and animals. For example, in murine models, scFOS shows several immunomodulating functions (13). Recently, we showed that scFOS administration enhanced the secretion of murine intestinal immunoglobulin A (8), which is expected to inhibit infection by pathogens. The change in murine intestinal microbiota due to scFOS administration is suspected to be a trigger of immunomodulating functions (8), although the mechanisms are still unclear. Comparison of the timing and dose response between changes in murine intestinal microbiota and immunomodulating functions should give us important information on the mechanisms of scFOS immunomodulating functions. For such purposes, it is necessary to determine the markers of change in murine intestinal microbiota after scFOS administration.

* Corresponding author. Mailing address: Food and Health R&D Laboratories, Meiji Seika Kaisha, Ltd., 5-3-1 Chiyoda, Sakado-shi, Saitama 350-0289, Japan. Phone: 81 492847592. Fax: 81 492847598. E-mail: koichiro_murashima@meiji.co.jp.

† These authors contributed equally to this work.

Effects of scFOS administration on murine intestinal microbiota have not been well characterized, although the effects on human intestinal microbiota have been studied intensively (17, 20). In the case of humans, fecal bacteria are cultured on selective media to determine the effects of scFOS administration on intestinal microbiota. This technique showed that an increase in the number of bifidobacteria had a major effect on human intestinal microbiota after scFOS administration. Based on these results, the CFU of bifidobacteria are utilized as a marker of the positive change in human intestinal microbiota after scFOS administration. In contrast, no consistent effects of scFOS administration on intestinal microbiota have been detected by the culturing method in the murine model (8). Therefore, no markers of change in murine intestinal microbiota after scFOS administration have been identified so far. Salzman et al. estimated that at least 60% of murine intestinal bacteria are still uncultured (18). In this context, the culturing method might not be suitable to determine changes in murine intestinal microbiota.

Molecular techniques are becoming popular to comprehensively determine intestinal microbiota (21). Most of the molecular techniques used to identify bacteria are based on the determination of 16S rRNA gene amplicons by PCR with universal primers. After PCR, the composition of the amplicons is determined by fingerprint analysis, such as terminal restriction fragment length polymorphism (T-RFLP), denaturing gradient gel electrophoresis, and temperature gradient gel electrophoresis. These molecular techniques allow access to uncul-

tured bacteria, since the DNA template for PCR is extracted directly from samples without bacterial cultivation. Therefore, these molecular techniques are powerful methods to detect the effects of scFOS administration on murine intestinal microbiota in which most bacteria are still uncultured.

In this study, we determined the effects of scFOS administration on the T-RFLP profiles of murine intestinal microbiota and sought markers for the positive change in murine intestinal microbiota as a result of scFOS administration.

MATERIALS AND METHODS

Animals. Female 6-week-old BALB/c mice (n = 7 for each diet group; Clea Japan, Tokyo, Japan) were housed at 23 to 25°C and 50 to 60% relative humidity with a 12-h light-dark cycle. The mice were fed a pelleted mouse flat diet (Oriental Yeast, Tokyo, Japan) for 1 week before commencement of the experimental diet. All experiments were performed in accordance with the Nihon University guidelines for laboratory animal care.

Diets. Mice were fed one of four experimental diets (scFOS diet, kestose [GF2] diet, nystose [GF3] diet, or control diet) for 5 weeks. The control diet consisted of 200 g of casein, 532 g of cornstarch, 70 g of corn oil, 10 g of vitamin mixture, 35 g of mineral mixture, 50 g of cellulose, and 100 g of sucrose. For the scFOS diet, GF2 diet, or GF3 diet, 75 g of the sucrose in the control diet was substituted with 75 g of scFOS, GF2, or GF3. All components, with the exception of scFOS, GF2, and GF3, were obtained from Oriental Yeast (Tokyo, Japan). Vitamin and mineral mixtures were prepared according to the AIN-93 formulation (16).The scFOS consisted of 34% 1-kestose (GF2), 53% nystose (GF3), and 10% fructofuranosyl nystose (GF4) (14) that was supplied by Meiji Seika Kaisha, Ltd. (Tokyo, Japan). The GF2 and GF3 were also supplied by Meiji Seika Kaisha, Ltd.

Sampling of fecal and cecal samples. Fecal samples were collected before commencement of the experimental diet (0 weeks) and at 5 weeks after changing the mouse flat diet to the experimental diet (5 weeks). Four to five fecal pellets were collected from each mouse. Also, cecal contents were collected from mice in the GF2-fed group, the GF3-fed group, and the control group at 5 weeks. Each collected fecal or cecal sample was stored at −80°C until DNA was extracted.

Extraction of DNA from fecal and cecal samples. DNA was extracted from 50 mg of each collected fecal or cecal sample with the UltraClean Soil DNA isolation kit (Mo Bio Labs, Solana Beach, CA) according to the method described by Clement and Kitts (2), with some modifications. To efficiently degrade bacterial cell walls, 50 μl of cell lysing solution (60 mg/ml of lysozyme, 1 mg/ml of *N*-acetylmuramidase SG [Seikagaku Kogyo Ltd., Tokyo, Japan] in TE buffer) was added to the bead solution from the kit. Subsequently, 50 mg of each fecal or cecal sample was added to the bead solution and incubated at 37°C for 30 min. After incubation, DNA was extracted according to the manufacturer's instructions. The DNA yields from fecal and cecal samples were 228 ± 65 ng and 222 ± 38 ng, respectively.

T-RFLP analysis. To amplify partial 16S rRNA gene fragments, PCR was done utilizing DNA from the fecal sample and the universal primers 27F (5′-AGAGTTTGATCCTGGCTCAG-3′) and 1492R (5′-GGTTACCTTGTTACGACTT-3′) (11). The 27F primer was labeled with 6′-carboxyfluorescein at the 5′ end. Amplification reactions were performed in a total volume of 50 μl containing 5 μl of DNA, 1.25 U of Takara Ex *Taq* (Takara shuzo, Tokyo, Japan), 5 μl of Ex *Taq* buffer, 8 μl of deoxynucleoside triphosphate mixture (2.5 mM each), and 25 pmol of each primer. The PCR program was 95°C for 3 min, then 25 cycles of 95°C for 30 s, 50°C for 30 s, and 72°C for 90 s, followed by 72°C for 10 min. PCR products were purified with the MinElute PCR purification kit (QIAGEN, Valencia, CA) and then digested with MspI. Lengths of terminal restriction fragments (T-RFs) in digested PCR products were analyzed by the ABI PRISM 310 genetic analyzer (Applied Biosystems, Foster City, CA) in Genescan mode, with the GS-500 ROX and GS-1000 ROX internal standards as described previously (10). The obtained T-RFLP profiles were analyzed by BioNumerics software (Applied Maths, Ver 3.0, Austin, TX) as described previously (10). To remove background and small peaks, T-RFs whose relative areas were less than 3.0% of total area were deleted by setting the "Min. profiling," which is a criteria to remove background, at 3.0% on the "auto search band" command of the software. Bands ranging from 50 to 600 bp were used to construct average T-RFLP profiles.

Construction of average T-RFLP profiles. To standardize all of the obtained T-RFLP profiles, we calculated the relative area of each T-RF against the summation of total area of all obtained T-RFs in each profile. The total area of each T-RFLP profile was set at 100%; therefore, the summation of all relative areas in each profile was 100%. The average relative area of each T-RF in the scFOS-fed group or the control group was then calculated, and the averaged T-RFLP profiles of both feeding groups were constructed. The statistical differences of the relative T-RF areas were determined by paired two-sided Student's t test. A P value of <0.05 was considered significant.

Sequence and phylogenetic analysis of the 16S rRNA gene. To amplify partial 16S rRNA gene fragments, PCR was performed utilizing one of the fecal DNAs of the scFOS-fed group or the control group as a template and the universal primers 27F and 1492R as described above. The amplified PCR fragments were directly ligated into pCR2.1 (Invitrogen, San Diego, CA) by TA cloning techniques (7) and then transformed into One Shot INVaF′ competent cells (Invitrogen) to construct 16S rRNA gene libraries. Clones isolated from the libraries were used as templates for sequence analysis. In the scFOS-fed and control groups, 77 and 67 clones were isolated, respectively. The partial sequences of the 16S rRNA gene (*Escherichia coli* positions 27 to 519) in all of the isolated clones were determined by the dideoxy chain termination reaction with the universal primer 27F or 519R (5′-ACCGCGGCYGCTGGC-3′) (11). The 16S rRNA gene sequences were submitted to the BLAST search program of the National Center for Biotechnology Information (1) to find similar sequences. Also, the 16S rRNA gene sequences were aligned with the CLUSTALW (19) with reference sequences obtained from the RDP Select Sequence function (12) and GenBank. To check secondary structures of the 16S rRNA gene sequences and correct the alignment, Se-Al (15) was used. A phylogenetic tree was constructed by the neighbor-joining method (3).

Real-time PCR with primers specific for *Bacteroidetes*. The 16S rRNA partial gene sequences determined as described above were aligned with CLUSTAL-W (19). Two regions where the sequences of the class *Bacteroidetes* are well-conserved but different from other sequences were found. Based on these two sequence regions, we designed two primers specific for the class *Bacteroidetes*: MIBF, 5′-GGCGACCGGCGCACGGG-3′ (forward primer), MIBR, 5′-GRCCTTCCTCTCAGAACCC-3′ (reverse primer). The amplification reactions were carried out in a total volume of 50 μl, which consisted of 1 μl of fecal DNA, 25 μl of SYBR green PCR master mix (Applied Biosystems), and 24 μl of deionized water. The fecal DNA was diluted to 1/10 concentration with deionized water. The PCR program was 95°C for 10 min, then 30 cycles of 95°C for 20 s, and 65°C for 60 s with the real-time ABI PRISM 7000 PCR machine (Applied Biosystems). To determine the specificity of the primer set MIBF and MIBR, the amplification rate of 2 pg of the 16S rRNA gene plasmids described above were determined. The amounts of 16S rRNA genes of the class *Bacteroidetes* were shown as a relative amount against the standard fecal DNA. The standard fecal DNA was extracted from a fecal sample from a mouse of the scFOS-fed group at 5 weeks. The standard curve was calculated with the data from standard fecal DNA, which was diluted to 1/1, 1/10, 1/100, or 1/1,000 concentration with deionized water. The statistical differences between amounts of 16S rRNA genes were determined by the two-sided Student t test. A P value of <0.05 was considered significant.

Nucleotide sequence accession numbers. The partial 16S rRNA gene sequences from the unique clones were deposited in the DNA Data Bank of Japan (DDBJ). The accession numbers are shown in Fig. 1.

RESULTS AND DISCUSSION

Search for increasing T-RFs after scFOS administration as markers of positive change in intestinal microbiota. To find increasing T-RFs after scFOS administration, we constructed the average T-RFLP profiles of 16S rRNA genes from murine intestinal microbiota in the scFOS-fed groups and compared this profile with that of the control group. The average T-RFLP profiles of both groups at 5 weeks are shown in Fig. 2. Six T-RFs (83, 88, 93, 95, 215, and 475 bp) in the T-RFLP profiles were significantly larger in the scFOS-fed group than in the control group. Therefore, these T-RFs were selected as marker T-RFs for positive changes in intestinal microbiota after scFOS administration.

We attempted to assign these marker T-RFs to phylogenetic groups with information on the theoretical lengths of T-RFs derived from 16S rRNA of murine fecal microbiota and the phylogenetic positions of these 16S rRNA genes. The accession numbers and theoretical T-RF lengths of the obtained 16S